NRL Report 8413

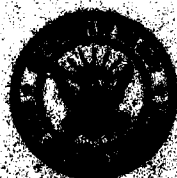# Experimental Measurements of Ambient Electromagnetic Noise from 1.0 to 4.0 kHz

ROBERT J. DINGER, WILLIAM D. MEYERS, AND JOHN R. DAVIS

Telecommunications Systems Technology Branch
Communications Sciences Division

July 31, 1980

(14) NRL8413   (12) 64

REPORT DOCUMENTATION PAGE	READ INSTRUCTIONS BEFORE COMPLETING FORM

1. REPORT NUMBER	2. GOVT ACCESSION NO.	3. RECIPIENT'S CATALOG NUMBER
NRL Report 8413	AD-A088090 (9)	

4. TITLE (and Subtitle)	5. TYPE OF REPORT & PERIOD COVERED
(6) EXPERIMENTAL MEASUREMENTS OF AMBIENT ELECTROMAGNETIC NOISE FROM 1.0 to 4.0 kHz	Final report on the NRL problem number
	6. PERFORMING ORG. REPORT NUMBER

7. AUTHOR(s)	8. CONTRACT OR GRANT NUMBER(s)
(10) Robert J. Dinger William D. Meyers, and John R. Davis	(17)

9. PERFORMING ORGANIZATION NAME AND ADDRESS	10. PROGRAM ELEMENT, PROJECT, TASK AREA & WORK UNIT NUMBERS
Naval Research Laboratory Washington, DC 20375	61153N; RR0210141 75-0200-0-0

11. CONTROLLING OFFICE NAME AND ADDRESS	12. REPORT DATE
Office of Naval Research Arlington, VA 22217	(11) 31 July 1980
	13. NUMBER OF PAGES
	63

14. MONITORING AGENCY NAME & ADDRESS(if different from Controlling Office)	15. SECURITY CLASS. (of this report)
(16) RR02101	UNCLASSIFIED
	15a. DECLASSIFICATION/DOWNGRADING SCHEDULE

16. DISTRIBUTION STATEMENT (of this Report)

Approved for public release; distribution unlimited.

17. DISTRIBUTION STATEMENT (of the abstract entered in Block 20, if different from Report)

DTIC

S ELECTE

AUG 20 1980

B

18. SUPPLEMENTARY NOTES

19. KEY WORDS (Continue on reverse side if necessary and identify by block number)
Very low frequencies
Extremely low frequencies
Radio noise
Noise excision techniques
Amplitude probability distributions

20. ABSTRACT (Continue on reverse side if necessary and identify by block number)
The spectral noise density, amplitude probability distribution (APD), and spectral content of ambient noise from 1.0 to 4.0 kHz were measured. Analysis of the recorded data included detailed investigation of the diurnal variation of the noise, comparison of the APDs with two atmospheric noise models, time-domain excision of noise impulses to assess the reduction in noise achievable by nonlinear processing, investigation of broadband ionospheric emissions identified as polar chorus, and determination of the statistical variation (in frequency) of the spectral minimum near 3 kHz. The analysis of the

(Continues)

251950

20. Abstract (Continued)

diurnal variation suggested the existence of a large propagation anisotropy in the nighttime earth-ionosphere waveguide at 3 kHz, with east-to-west attenuation significantly lower than north-south attenuation. The observed seasonal and geographical averaged diurnal variations can be interpreted qualitatively in terms of worldwide thunderstorm distributions and day-night changes in the reflecting height of the ionospheric D-layer. The measured spectral noise density values are significantly lower than values measured under similar conditions by earlier investigations; the lower values are attributed to the use of a receiver with a lower intrinsic noise and careful site selection to avoid man-made interference. The recorded APDs varied from a Rayleigh form during low noise periods in Norway to a distribution with a tail at low exceedence values during higher noise periods in both Norway and Italy. Comparison of the APDs with the Field-Lewenstein model and the Middleton model generally showed satisfactory agreement.

Processing of the recorded noise by clipping the large atmospheric noise impulses lowered the spectral noise density in Italy by an average of 6.7 dB (winter) and 3.3 dB (summer). The noise reduction in Norway was highly variable; usually little or no lowering was possible, but during one nearby summer thunderstorm a reduction of 26 dB was achieved. In Norway broadband emissions were observed on about 20 percent of the measurement days. No emissions were observed in Italy. The spectral content of the emissions and their diurnal variation identify them as polar chorus.

A distinct spectral minimum in the vicinity of 3 kHz was *always* observable in Norway but was frequently not observable in Italy. The statistical distribution of the frequency of the Norway minimum had a peak near 3.6 kHz.

ACCESSION for

NTIS	White Section	☑
DDC	Buff Section	☐
UNANNOUNCED		☐
JUSTIFICATION		

BY

DISTRIBUTION/AVAILABILITY CODES

| Dist. | AVAIL. and/or SPECIAL |
| A | | |

CONTENTS

EXPERIMENTAL MEASUREMENTS OF AMBIENT ELECTROMAGNETIC NOISE FROM 1.0 TO 4.0 kHz

SUMMARY

Measurements have been made at two carefully chosen sites in Italy and Norway of the spectral noise density, amplitude probability distribution (APD), and spectral content of ambient noise from 1.0 to 4.0 kHz. Analysis of the recorded data has included detailed investigation of the diurnal variation of the noise, including comparison between the two sites, between orthogonal directions at each site, and with meteorological data; comparison of the APDs with two atmospheric noise models; time-domain excision of noise impulses to assess the reduction in noise achievable by nonlinear processing; investigation of broadband ionospheric emissions identified as polar chorus; and determination of the statistical variation of the spectral minimum near 3 kHz. Our specific conclusions regarding each area of the data analysis are as follows:

- *Diurnal variation.* The analysis of the diurnal variation in Norway suggested the existence of a large propagation anisotropy in the earth-ionosphere waveguide at 3 kHz. An interpretation of this anisotropy in terms of an attenuation coefficient that is a strong function of the angle between the direction of propagation and the earth's magnetic field is supported by the theoretical calculations of Barr [1]. The diurnal variations at 3 kHz in general showed a larger ratio of the nighttime maximum value to the daytime minimum than did diurnal variations in other portions of the ELF and VLF bands and appeared to be more repeatable from day to day. Several days of abnormally high daytime noise-density values were attributed to nearby thunderstorms. The observed seasonal and geographical averaged diurnal variations were interpreted qualitatively in terms of worldwide thunderstorm distributions and day-night changes in the ionospheric D-layer reflecting height. Our measured values of the spectral noise density were significantly lower than values measured under similar conditions by earlier investigations; we attribute our lower values to the use of a receiver with a lower intrinsic noise and careful site selection to avoid man-made interference. Noise spectral densities in Norway varied from -192 dBH (mean daily minimum in March 1978) to -184 dBH (mean daily maximum in March 1978) and in Italy varied from -187 dBH (mean daily minimum in March 1978) to -160 dBH (mean daily maximum in June 1978), where dBH is dB relative to 1 A/m$\sqrt{\text{Hz}}$.

- *APD results.* The recorded APDs varied from a Rayleigh distribution during low noise periods in Norway to a distribution with a pronounced tail at low exceedence values during higher noise periods in both Norway and Italy. Comparison of the APDs with the Field-Lewenstein model [2], which is phenomenological propaga-

tion-oriented formulation, and the Middleton model [3], which is a canonical source-oriented formulation, generally showed reasonable agreement. The temporal variations of the model APD parameters derived by fitting the experimental APDs to both the Field-Lewenstein and Middleton APD equations were consistent with known source and propagation conditions, and the fitting assisted in interpreting the diurnal changes in the noise spectral density. The Field-Lewenstein probability density function and APD, we conclude, are satisfactory closed-form expressions that could be of use in further efforts to optimize waveforms and predict the communication performance of a 3-kHz tactical communication system.

- *Noise processing.* Clipping of the large atmospheric noise impulses lowered the effective spectral noise density by an average of 6.7 dB in Italy in March 1978 and 3.3 dB in Italy in June 1978. In Norway there was usually little or no noise reduction, since the noise was nearly Gaussian to begin with, but at an exceptional time during a nearby thunderstorm in June 1977 a reduction of 26 dB was achieved. The best clipping bandwidth was measured to be about 140 Hz, and the clipping performance was found to be relatively insensitive to the clipping level (within limits).

- *Ionospheric emissions.* In Norway broadband emissions were observed on about 20% of the measurement days. No emissions were observed in Italy. From the spectral content of the emissions and their diurnal variation they were identified as polar chorus. A particularly intense and long-lived event occurred on 26 March 1978. The APDs of the emissions were Rayleigh, as expected for a broadband and noiselike process, and no significant reduction in spectral noise density was possible by clipping.

- *Spectral minimum variation.* A distinct spectral dip in the vicinity of 3 kHz was *always* observable in Norway but was frequently not observable in Italy. The statistical distribution of the frequency of the Norway minimum had a peak near 3.6 kHz, which value was attained nearly 30% of the time.

INTRODUCTION

This report describes the results of a 2-year program to characterize the statistical and synoptic properties of ambient electromagnetic noise in the band from 1.0 to 4.0 kHz. The emphasis of the program has been to measure those characteristics of the noise that most strongly influence the design of potential naval communication systems in this frequency band. The dominant contribution to ambient electromagnetic noise in the extremely-low-frequency (ELF, 3 Hz to 3 kHz) and very-low-frequency (VLF, 3 to 30 kHz) bands arises from atmospheric noise generated by lightning strokes in thunderstorms. Radiation from the strokes propagates in the earth-ionosphere waveguide to great distances, so that the ELF and VLF noise measured by a receiver on the earth's surface is a superposition of propagation-modified lightning-stroke radiation from throughout the world. Near 3 kHz, the propagating waveguide modes become cut off, and all modes become highly attenuated. The actual modal cut off frequency for a nonideal ionosphere depends on the details of its structure and varies according to time of day, latitude, and season. Usually the range of frequencies from about 2 to 4.5 kHz is considered as the cutoff band; because of the high

attenuation in this band, atmospheric noise has a minimum value. It is this low-ambient-noise spectral density and the prospect of a localized, controllable propagation range that make a communication system operating in the attenuation band attractive for such applications as tactical submarine communications. Appendix A summarizes briefly the key features of VLF propagation with particular emphasis on the modal cutoff band.

Previous measurements of ambient noise from 1 to 4 kHz (which are summarized below) are sparse and are not useful for providing the information required to assess the feasibility of a 3-kHz communication system. In particular the following additional data are required:

- Long term seasonal and diurnal variations of the noise spectral density.

- Noise reduction by time-domain excision. It has been demonstrated [4] at ELF that clipping of the atmospheric noise impulses can significantly decrease the effective noise spectral density. Data are required on the expected improvement at 3 kHz.

- Amplitude probability distribution (APD). Efficient design of signaling formats and modulation schemes requires knowledge of statistical noise functions such as the APD. No APDs for noise in the attenuation band have been reported.

- Meteorological influences on 3-kHz noise. Because of the high attenuation rate, local thunderstorms have a proportionally larger effect on the properties of noise from 1 to 4 kHz than they do in the rest of the ELF and VLF bands. Measurements of this influence are required.

Measurements were taken at a midlatitude site (Giglio Island, Italy) and an auroral-zone site (Tromsø, Norway) during approximately 125 days during the winter and summer. The data recording consisted of broadband tape recording of noise in the entire band from 1.0 to 4.0 kHz, narrowband tape recording (at increased sensitivity) of noise in a 150-Hz bandwidth centered near 3 kHz, strip-chart recordings of the RMS noise density near 3 kHz, and real-time computation and recording of the APD. The magnetic field of the noise was sensed using air-core loop antennas; two orthogonal antennas were employed to obtain measurements of the directional characteristics of the noise. Analysis of the recorded data included the generation of time-spectral plots to reveal spectral features of the noise, time-domain excision of noise impulses to assess the reduction in noise achievable by non-linear processing, comparison of the APDs with the Field-Lewenstein [2] and Middleton [3] noise models, and comparison of the noise features with meteorological and geophysical data.

The outline of this report is as follows. After discussing previous noise measurements in this frequency band, we will describe the antennas, receiver, and data-recording electronics. We will then discuss the observed diurnal variations of the noise and relate a number of specific features of the variation to meteorological conditions and to propagation in the earth-ionosphere waveguide. We will next discuss the recorded APDs and compare them with several general atmospheric noise models. Then we will describe the noise-processing experiments in which we clipped the large noise impulses and measured the reduction in the

3

noise spectral density. After briefly describing some features of several ionospheric emission events observed in Norway, we will analyze the variation of the minimum-noise-density frequency. We will finish with recommendations for further measurements.

PREVIOUS MEASUREMENTS OF 3-kHz NOISE

The first measurements to show that lightning-stroke spectra have an appreciable energy in the ELF and lower VLF bands were by Appleton and Chapman [5] in 1937. The first quantitative measurements of spectral noise density in these bands were not made until 1957, when Watt and Maxwell [6] made measurements over a wide range of latitudes from 1 to 10 kHz; other measurements [7-11] of noise in the ELF and lower VLF bands were made in the late 1950s and early 1960s. However, the noise levels reported in Refs. 6 through 11 for the attenuation-band minimum are too high and indicate contamination by man-made noise, lack of sufficient sensitivity in the receiver, or both. The depth of the attenuation band in the spectra observed in 1965 by Westerlund [12] in Kiruna, Sweden, suggests that his measurements were generally reliable and uncontaminated, but his spectra are uncalibrated. These early measurements emphasize the need for a carefully designed receiving system using low-noise amplifiers in the first stages of amplification and the need to select measurement sites that are remote from power lines and other sources of man-made interference. Also clear from these earlier measurements is that an air-core loop antenna is easier to calibrate than and maintains its calibration better than either a vertical whip antenna or a permeable-core loop antenna.

Feltham [13] presents a study of radio noise in a frequency range 200 Hz to 10 kHz that is probably the most thorough investigation of the diurnal variation of noise in this band. His technique consisted of using a single air-core loop antenna with an external shunt capacitor that was varied in discrete steps by a stepping motor to tune the loop to six frequencies across the band. This technique permits a low noise level at each discrete frequency, because the loop is tuned, but does not give simultaneous noise measurements. Time and frequency resolution is necessarily coarse. Feltham took only strip-chart recordings of the noise spectral densities. Our spectral density results will be compared with those by Feltham later in this report.

The various types of discrete and broadband emissions of ionospheric and magnetospheric origin that occur throughout the VLF band are sometimes observable near 3 kHz. Helliwell [14] has summarized these emissions and the measurements of their characteristics made up to about 1965, and Ref. 15 refers to more recent measurements.

EXPERIMENTAL PROCEDURES AND EQUIPMENT

Table 1 gives information about the two sites at which attenuation-band ambient-noise data was gathered and also lists the intervals of data presented in this report. Figure 1 is a block diagram of the receiver and recording equipment used at the Norway and Italy sites during the coordinated 1978 measurements. The configuration shown in Fig. 1 evolved on the basis of experience obtained during the three earlier (1976 and 1977) observation periods listed in Table 1. For discussion the system shown in Fig. 1 can be divided into three subsystems: antenna and amplifier, signal conditioning and recording, and the amplitude-probability-distribution (APD) computer.

4

Table 1 — Where, When, and How We Measured
the Attenuation-Band Wide-Band Noise

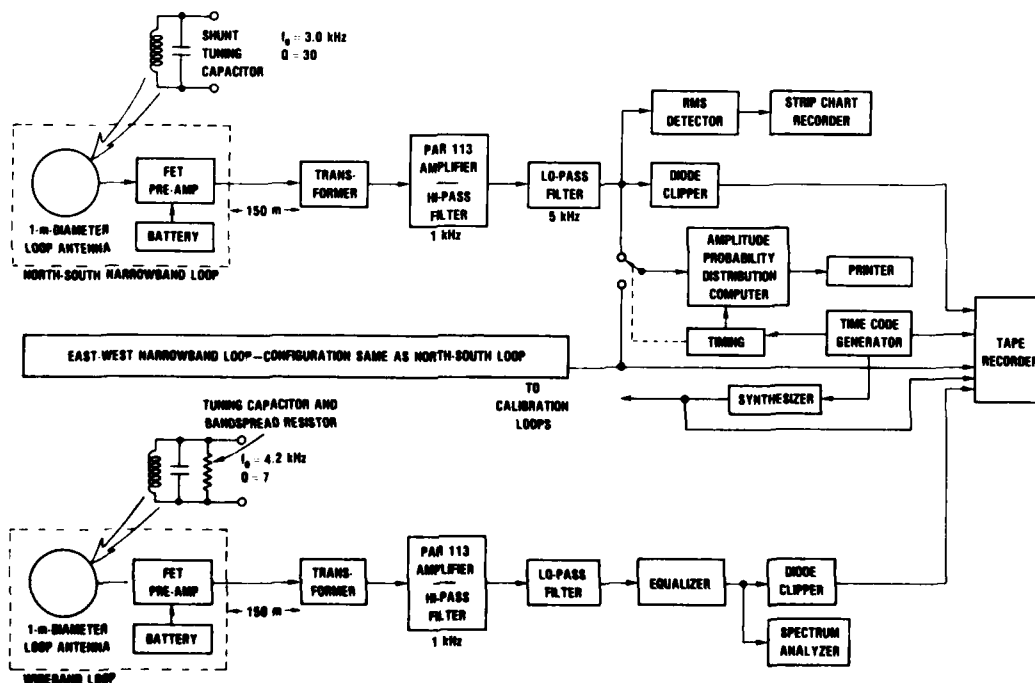| Data Interval	Number of Loop Antennas		Use of an Amplitude-Probability-Distribution (APD) Computer	Use of an On-Line Spectrum Analyzer
	Wideband	Narrowband		
Site at Tromsϕ, Norway, with geographic coordinates 19°E, 70°N and magnetic coordinates 118°E, 67°N				
8-11 Aug. 1976	2	0	No	No
9-16 Jan. 1977	2	0	Yes	Yes
8-28 June 1977	1	1	Yes	Yes
12 Mar. to 4 Apr. 1978	1	2	Yes	Yes
7-30 June 1978	1	2	Yes	Yes
Site at Giglio Island, Italy, with geographic coordinates 11°E, 42°N and magnetic coordinates 90°E, 42°N				
16 Mar. to 4 Apr. 1978	1	2	Yes	No
9-28 June 1978	1	2	Yes	No

Fig. 1 — Receiver and recording electronics

Antenna and Amplifier

Although electric monopole and dipole whip antennas have been used to measure 3-kHz ambient noise [6,9], the absolute calibration of a whip antenna is difficult to maintain at 3 kHz because of the variable electrostatic effects of precipitation, wind, and humidity. We chose to use air-core loop antennas because of their good long-term stability. A ferrite-core loop antenna would permit a physically smaller antenna than an air-core loop antenna with the same sensitivity, but the presence of the core makes the antenna more difficult to calibrate, and stressing of the core can cause the calibration to vary.

The antenna developed for the noise measurements (Fig. 2) consists of 350 turns of No. 14 wire wound on a plywood form 1 meter in diameter. Also shown in Fig. 2 is a single-turn calibration loop. Three loop antennas were used at each field site.

Two of the antennas were tuned with a shunt capacitance to a center frequency of 3.0 (± 0.1) kHz, with a 3-dB noise bandwidth of 150 Hz. These two antennas, one oriented geographically north and south and the other geographically east and west, were used to obtain the RMS noise spectral densities, data for the clipping analysis, and the APD-computer inputs. The narrowband tuning was required to obtain the lowest possible intrinsic antenna noise. According to Watt [16] the intrinsic antenna noise referred to an equivalent input magnetic field is given in $A/m\sqrt{Hz}$ by

$$H_n = 4.03 \times 10^{-8} \sqrt{\frac{k}{fQ}} \frac{F_v}{A^{3/4}} , \qquad (1)$$

where k is the loop inductance factor (available in graphical form in Ref. 16), F_v is the noise factor of the preamplifier, f is the frequency, $Q = \Delta f/f$, with Δf being the 3-dB noise bandwidth, and A is the loop area. The receiver noise factor is given by

$$F_v = \sqrt{1 + (R_{eq}/Q^2 R_a)}, \qquad (2)$$

where R_a is the effective loop resistance and R_{eq} is the equivalent input noise resistance of the preamplifier. Equation (2) displays the principal reason for using a tuned loop: a substantial reduction in the value of F_v is possible for a large value of Q.

The preamplifiers used two low-noise field-effect transistors (type 2N6550) in a push-pull configuration to drive a balanced line through a transformer. The average equivalent noise resistance of the preamplifier was 250 ohms. Substituting in Eq. (1) the values $k = 2.2$, $f = 3 \times 10^3$ Hz, $Q = 30$, $A = 0.79$ m^2, $R_{eq} \approx 250$ ohms, and $R_a = 64$ ohms yields $H_n = -195.5$ dB//1 $A/m\sqrt{Hz}$ as the expected equivalent magnetic field noise level for the tuned antenna and preamplifier. (In the remainder of this report dB//1 $A/m\sqrt{Hz}$ will often be abbreviated as dBH. Signal levels will be given as dB//1 A/m and will often be abbreviated as dBA/m.)
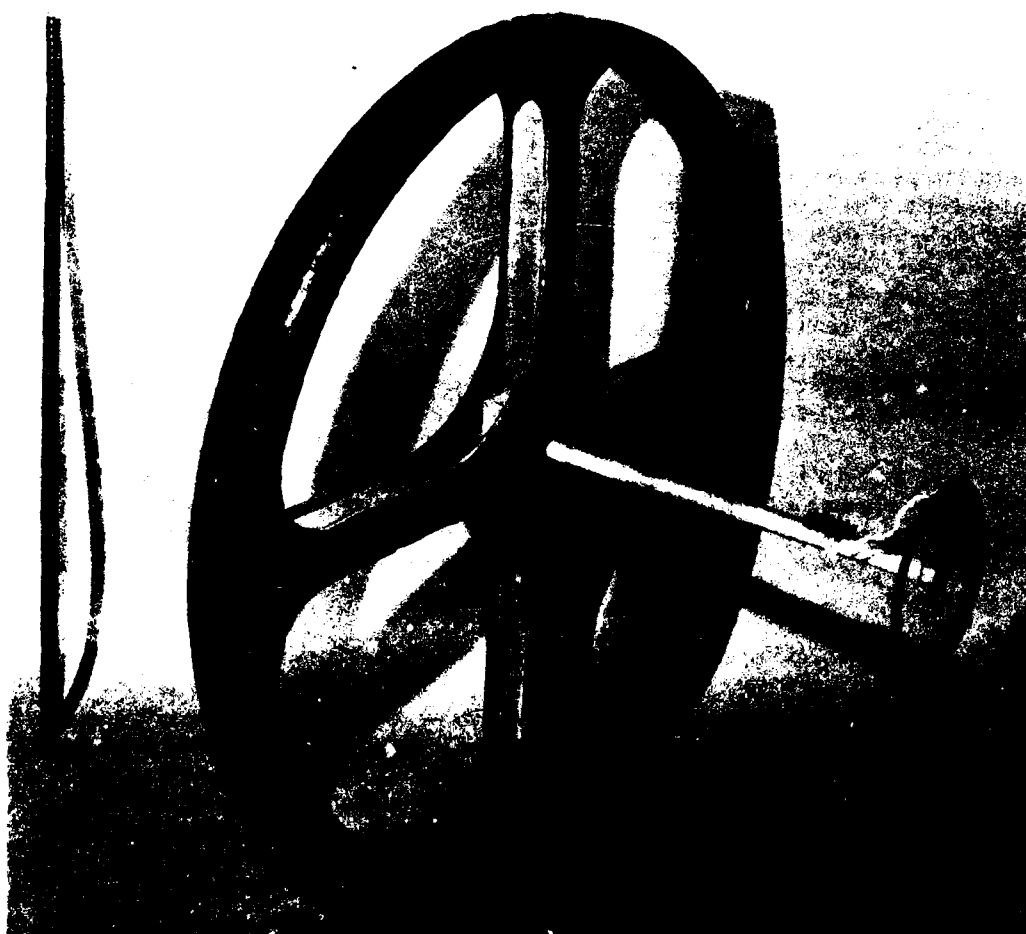
6

Fig. 2 — 3-kHz loop antenna with calibration coil

The actual antenna noise, as measured in a shielded room that was specifically designed to attenuate VLF noise, was about –193 dBH. However, at 3 kHz some external noise was probably present in the shielded room at this level, and the actual antenna plus preamplifier noise may be closer to the expected –195-dBH value.

The third antenna at each site was a broadband antenna whose purpose was to measure the ambient noise over a bandwidth from 1.0 to 4.0 kHz for spectral analysis. As shown in Fig. 1, this antenna was resonated at 4.2 kHz with a low Q value by using a shunt capacitor and resistor, giving a 3-dB bandwidth for the antenna and preamplifier of about 1 kHz. This low Q tuning of the antenna in conjunction with the natural 6-dB-per-octave increase in loop response with increasing frequency, the 1-kHz high-pass filter in the postamplifier, a 2-kHz low-pass filter, and an equalizer shaped the overall response to be flat between 1.0 and 4.0 kHz. Within this bandwidth the system noise was measured in the shielded room to be at least –189 dBH.

For completeness and for a more thorough analysis of the data a second broadband loop would have been desirable in order to measure the spectral features of the noise in two orthogonal directions. However, we were limited to three data channels by the battery-operated tape recorder at the Italian site. Most of the time the broadband loop at each site was oriented in a geographic north-south direction.

All loops had a copper-foil electrostatic shield wound as a toroid around the turns of the loop. The loops were installed in the open, since wind screens were found to be un-necessary, with a plastic tarp around them for protection from the weather. The pre-amplifiers were located at the loops and were powered by batteries.

Signal Conditioning and Recording

Particular care was taken in the design of the signal conditioning and recording tech-niques to maintain as large a dynamic range as possible throughout the chain of amplifiers and filters, clipping only when necessary. Ambient noise within the 3-kHz attenuation band has a larger dynamic range than ELF or VLF noise below and above the band because of the high attenuation of noise impulses from distant thunderstorms and low attenuation of the impulses from nearby thunderstorms.

As shown in Fig. 1, the signal from the 150-m cable was passed into a combination postamplifier and high-pass filter with a corner frequency of 1 kHz. In the Norway measure-ments Princeton Applied Research (PAR) 113 amplifiers were used, but in Italy amplifiers designed and constructed by NRL were used. The signals from the two narrowband loops were then passed through a low-pass filter with a corner frequency of 5 kHz and steep 42-dB-per-octave skirts.

8

After the two narrowband signals were filtered, they went to three processing/ recording devices: a tape recorder, an RMS detector and strip chart recorder, and an APD computer. Prior to recording on the tape recorder, the noise was clipped at a level of -130 DBA/m with a diode clipper to prevent overdriving of the recorder. The dynamic range on the tape recorders in the 150-Hz bandwidth was measured to be approximately 65 dB for the recorders at both sites. The RMS detector was designed around an Analog Devices 4340 RMS voltage converter; the RMS voltage was recorded on Esterline-Angus strip chart recorders. The APD computer, which was time-shared between the two narrowband signals, will be described in the next subsection.

The wideband signal, after having its spectral response shaped as described, was clipped and recorded on the tape recorder. In Norway a portable spectrum analyzer was available to monitor the spectrum.

We calibrated the loop antenna by injecting a sine wave from a function generator into a single-turn calibration loop mounted on the antenna frame (Fig. 2). We used the procedure and equations given by Jean et al. [17]. For the determination of the effective noise levels produced by clipping of the atmospheric noise impulses (described in a later section), a continuous reference tone at a low level had to be injected at the loop. This injected tone served as a pilot signal for the lock-in detectors required in the clipping analysis. This signal was injected at a level of about -188 dBA/m in Italy and -196 dBA/m in Norway.

APD Computer

The APD is a measure of the percentage of time during an observation interval that the noise amplitude exceeds a given level. The APD is usually plotted as a curve of exceedence values (either in percentage or as a fraction) on one axis as a function of noise amplitude. For ELF and VLF noise the interesting features of the APD occur at the low exceedence values, that is, at the high values of noise amplitude that are exceeded a small fraction of the time. Therefore it is important that the APD be determined at a point where little or no clipping of the noise impulses has occurred. In the previous subsection we indicated that the input to the tape recorder must be clipped at -130 dBA/m to avoid saturation of the recorder electronics. However, an appreciable percentage of the atmospheric noise impulses exceed this value; hence calculation of the APD from the tape-recorded noise would give inaccurate results at the low exceedence values. Hence we designed and fabricated a hybrid analog-digital computer for real-time determination of the APD at point in the circuit where essentially none of the noise impulses were clipped.

Figure 3 is a block diagram of the APD computer. The accumulators measure the total time that a preset value of noise amplitude is exceeded in a time interval controlled by the sequencer. We used a measurement interval of 2 minutes in all of our measurements. Figure 4 shows a schematic diagram of an accumulator. Amplifier A1 is driven open loop as a voltage comparator, with an adjustable reference level. When the input voltage equals the reference voltage, the output of A1 goes high and stays high until the input voltage drops below the reference voltage. Transistor Q1 is a switch that inhibits A1 except during the 2-minute accumulation period determined by the sequencer. The output of A1 is applied to A2, which is an integrator. Transistor Q2 serves to reset the integrator to zero just prior

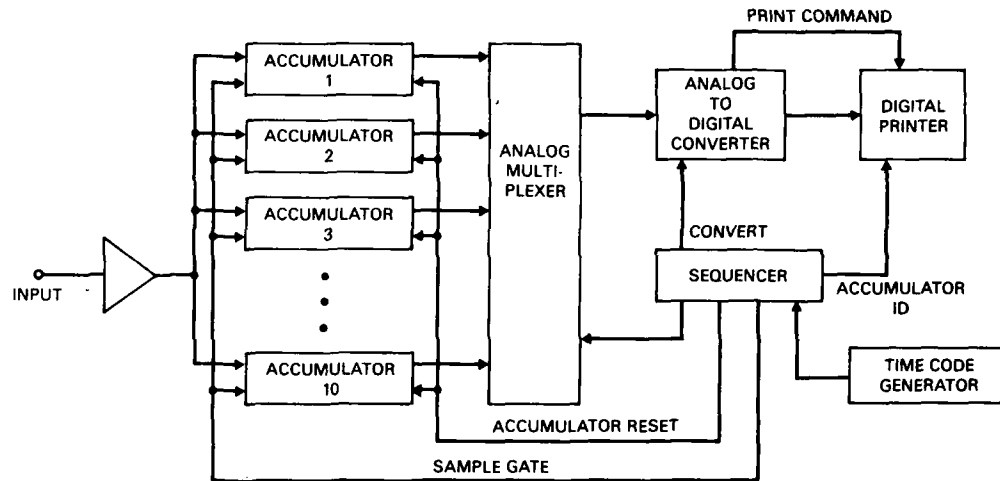Fig. 3 — APD computer
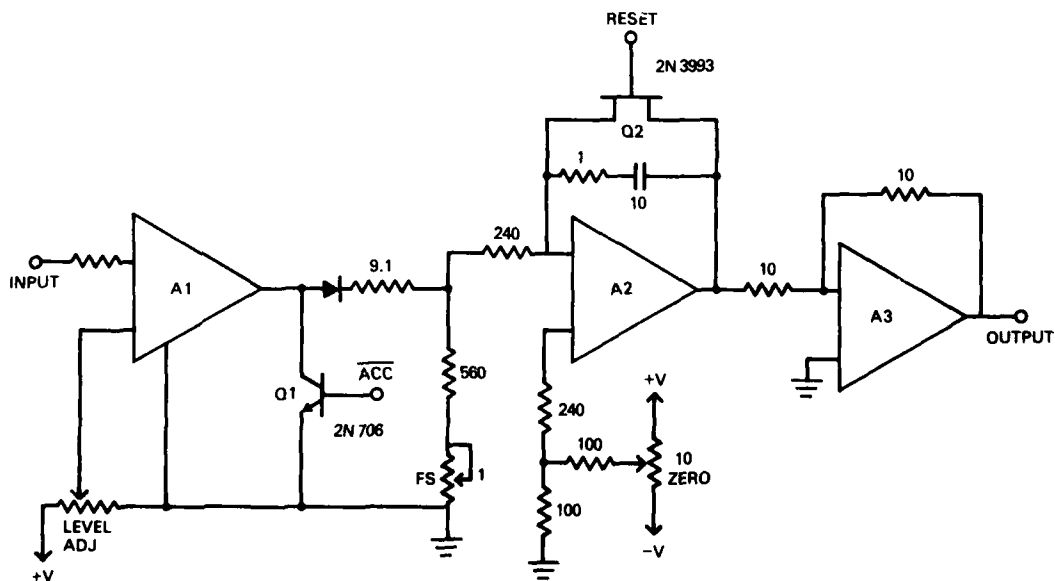

Fig. 4 — APD accumulator

to the accumulation period by means of a pulse received from the sequencer. At the end of the 2-minute accumulation period, the voltage at the output of A2 is proportional to the amount of time the reference voltage was exceeded. Amplifier A3 is a buffer for the integrator.

As shown in Fig. 3, the accumulator output voltages are passed (on command from the sequencer) into an analog-to-digital converter and printed on a digital printer. Although a digital tape recorder would have considerably eased the subsequent analysis of the APD data, considerations such as reliability and power consumption favored a digital printer.

The reference level for accumulator 1 was set to a voltage corresponding to an input magnetic-field amplitude of -123 dBA/m in Norway (for both the March 1978 and June 1978 measurements) and in Italy of -117 dBA/m for the March 1978 measurements and -113 dBA/m for the June 1978 measurements. These various levels for accumulator 1 reflected the peak atmospheric noise levels prevailing at the time. Each successive accumulator had its reference level set 6 dB lower in amplitude than the preceding accumulator; thus, for example, in Norway the accumulators spanned a range from -123 dBA/m to -177 dBA/m.

The APD computer was time-shared between the two narrowband loops as shown in Fig. 1. An APD was printed out every 10 minutes, based on 2 minutes of observation time; since the input switched between the two orthogonal loops on every APD, one APD is available every 20 minutes for each of the two orthogonal directions.

Direction Finding

In Norway periodic measurements of the azimuthal arrival angle of atmospheric noise impulses were made by applying the outputs of the two orthogonal narrowband receivers to the inputs of an oscilloscope operating in an xy mode. During the calibration period that began each tape, a phase-coherent sine wave was injected into both the east-west and north-south loops, and the x-axis and y-axis gains on the oscilloscope were adjusted so that a $45°$ line appeared on the screen. The resulting Lissajous figure was always a line, indicating negligible phase distortion in either antenna.

To record the impulse arrival angle, an oscilloscope camera was exposed for an interval of time, typically about 20 seconds. When the impulses during the interval were well separated and nearly linearly polarized, their arrival angle was easily observed on the photograph, as shown in several cases in this report. However, when the impulses were elliptically polarized or activity was high, it was sometimes difficult to determine an arrival angle.

Most of our direction-finding measurements were done at the Norway site while the data were being recorded. This procedure allowed the highest possible dynamic range.

DIURNAL VARIATION

The diurnal variation of atmospheric noise in the ELF and VLF bands is a result of diurnal changes both in the source characteristics (the intensity and distribution of thunderstorms) and in the propagation. Typically at midlatitudes the noise spectral density attains its lowest value during the daytime (usually during the local morning hours), when the higher daytime attenuation rates and decreased thunderstorm activity combine to produce a low value. The noise spectral density usually attains its highest value during the early evening hours because of enhanced thunderstorm activity and a lower nighttime attenuation rate.

This section presents the measured diurnal variations for atmospheric noise as measured by the narrowband tuned loops (Fig. 1). We have been able to interpret most of the features of the diurnal variations qualitatively, knowing the general locations of thunderstorm centers (and, in several cases, specific locations of nearby storms) and knowing the general features of 3-kHz propagation. A more quantitative comparison of the diurnal noise variation using, for example, computer-generated noise models based on assumed thunderstorm distributions, source models, and propagation equations does not appear to be required.

Data

The complete diurnal-variation plots of the RMS spectral noise density at 3.0 kHz are shown in Figs. 5, 6, and 7. Figure 5 shows the data taken during June 1977 in Norway; only one narrowband loop was available then, and this loop was oriented to measure north-south noise for 11 days and then rotated to east and west for about 4-1/2 days. Figures 6 and 7 display the March 1978 and June 1978 data respectively for both the east-west and north-south loops in a manner designed to facilitate comparison between the Norway and Italy sites. Also shown on these figures are the periods of local day and night, both on the ground and in the ionosphere at a height of 70 km. Several other items to be discussed in detail later, such as suspected emission events and occurrences of local thunderstorms, are also indicated on the figures.

Figures 8, 9, and 10 are plots of the average diurnal variation for the three measurement periods. These graphs help to show the overall shape and features of the variation in the spectral noise density.

General Features

Under conditions of sunrise and sunset at the site (the March measurements at both sites and the June measurements in Italy), the spectral density variation shows the expected daytime low, a substantial increase in noise density at sunset, a peaking of the noise density at local midnight, a slow decrease in noise during the remainder of the local nighttime hours, and a decrease in noise at sunrise. The diurnal variation is more pronounced at the Italian site than at the Norwegian site for the March data, presumably because of the smaller distance to a major thunderstorm area (central Africa). During the times no day-night terminator passed over the Norwegian site (as was the case during the times of all of the
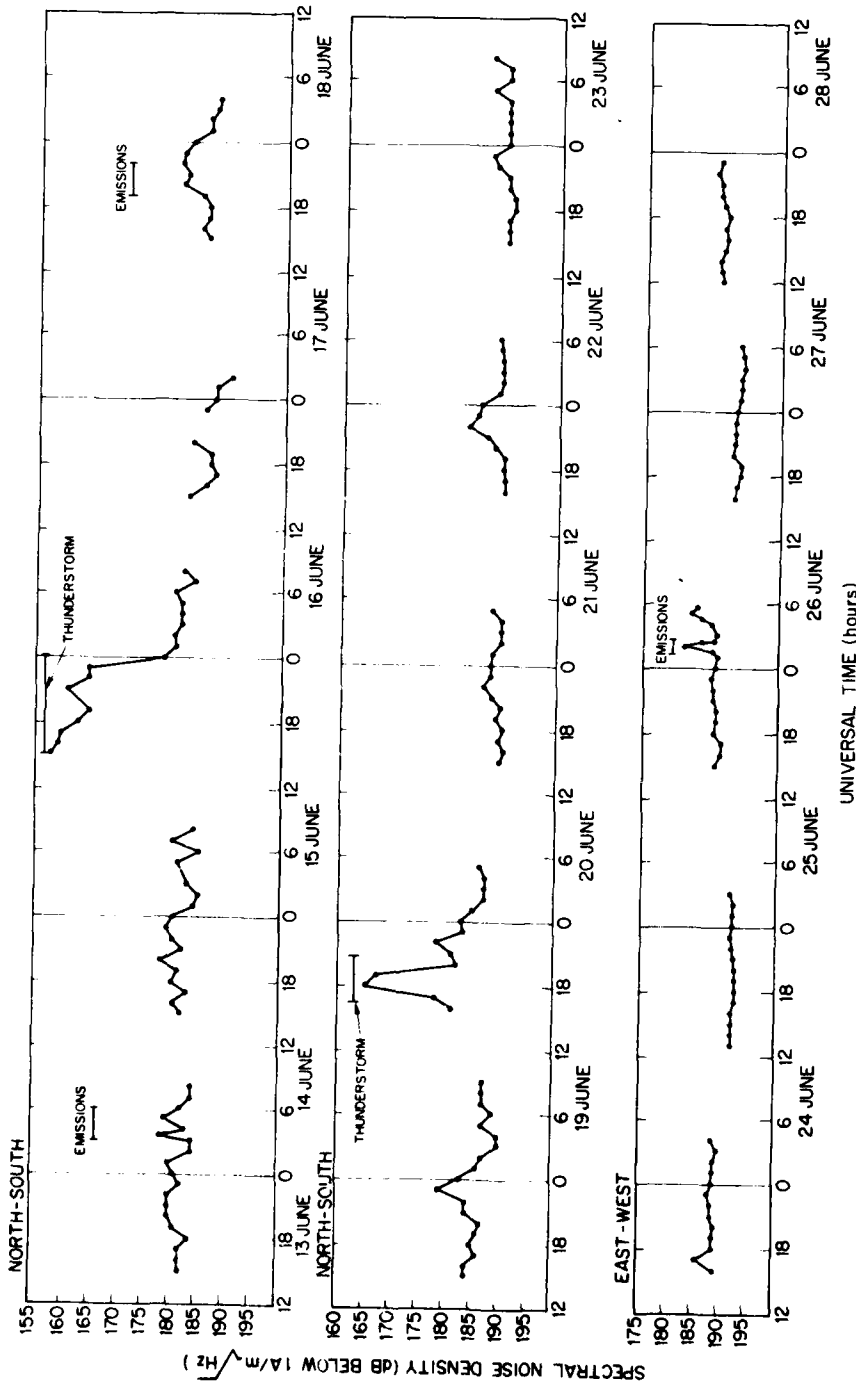
Fig. 5 — Diurnal variation in Norway of the noise spectral density at 3 kHz during June 1977. The loop antenna from which the noise values are derived was oriented geographically north and south from 12 June to 23 June and was rotated to east and west from 23 June to 30 June.
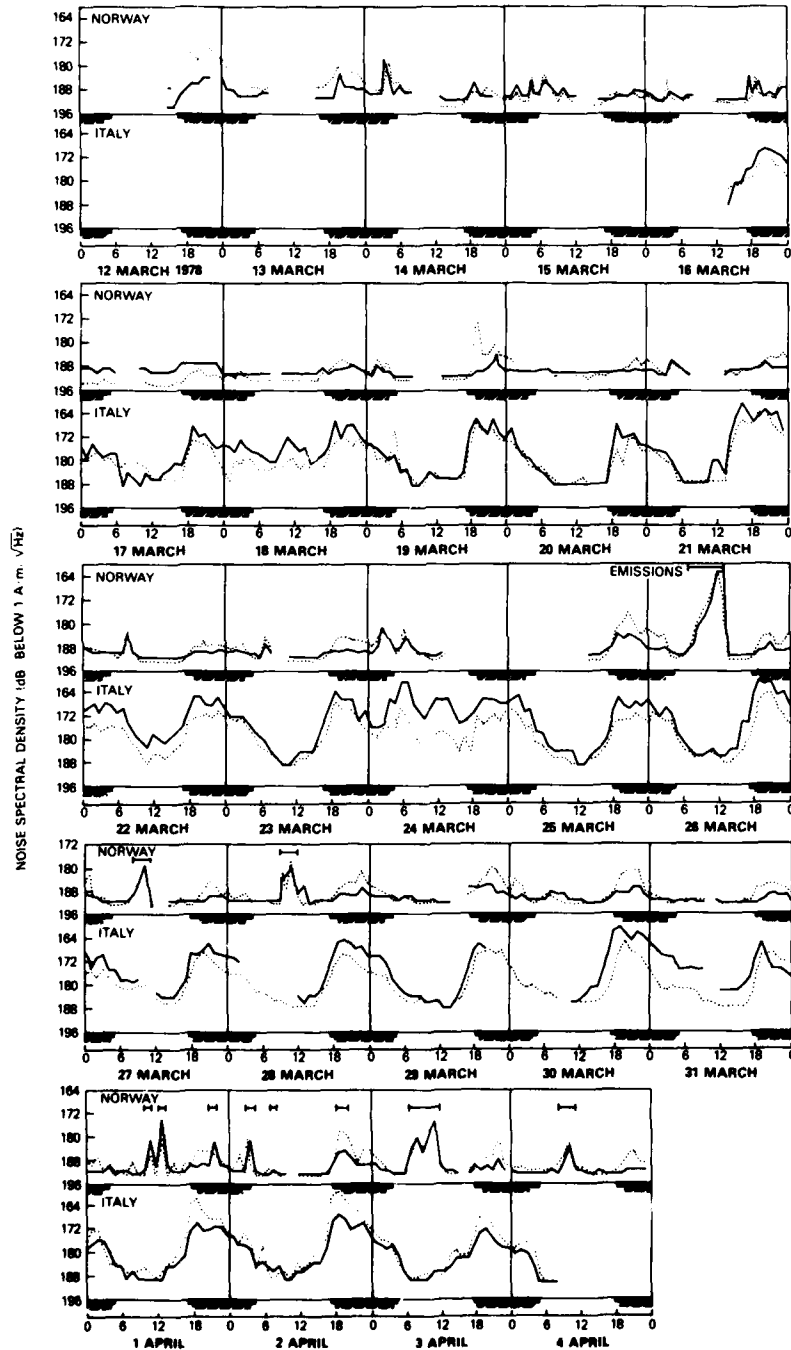
13

Fig. 6 — Diurnal variation of the noise spectral density at 3 kHz between
12 March 1978 and 4 April 1978 as measured in Norway and Italy. The
north-south loop is shown with a solid line, and the east-west loop is
shown with a dashed line. The solid bars indicate periods of surface night-
time, and the hatched bars indicate periods of ionospheric nighttime at
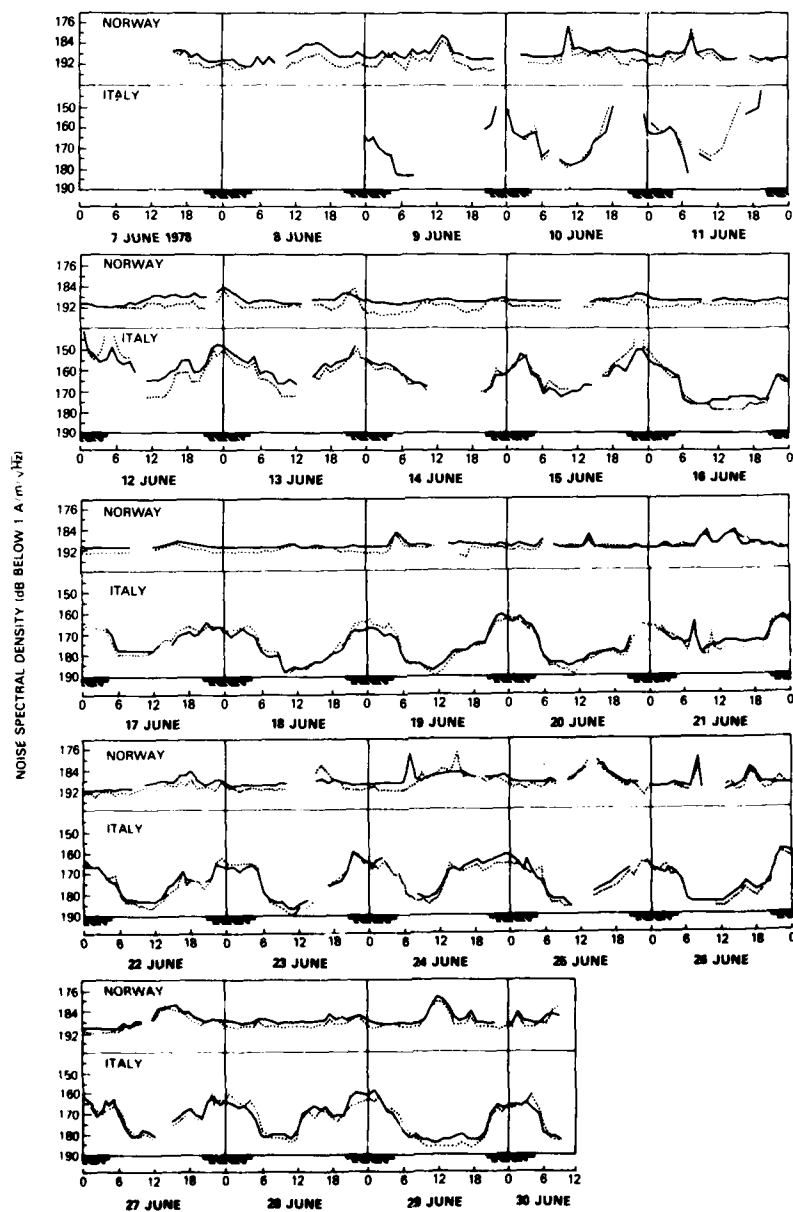a height of 70 km.

14

Fig. 7 — Diurnal variation of the noise spectral density at 3 kHz between 7 June 1978 and 30 June 1978 as measured in Norway and Italy. The north-south loop is shown with a solid line, and the east-west loop is shown with a dashed line. The solid bars indicate periods of surface nighttime, and the hatched bars indicate periods of ionospheric nighttime at a height of 70 km.
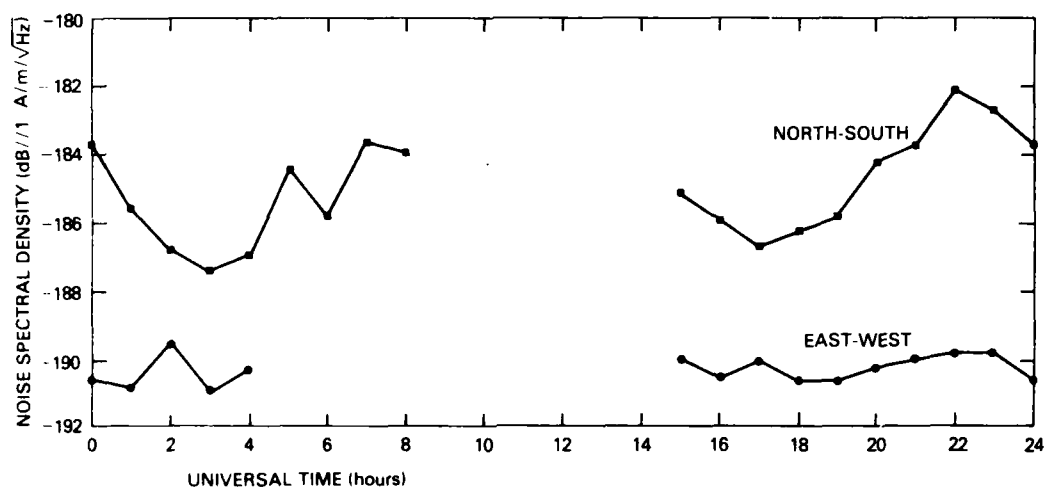
15

Fig. 8 — Average diurnal variation of the noise spectral density in June 1977 as measured in Norway. The north-south and east-west points were not recorded simultaneously.

June 1977 and 1978 data), relatively little consistent diurnal variation is observed. The large increases in the noise level on 15 June 1977 and 19 June 1977 in Fig. 5 were caused by local thunderstorms; these thunderstorms will be discussed later in conjunction with the results of nonlinear noise processing.

Generally the north-south noise level is higher than the east-west noise level in Italy during the times of both the March and June data, although the difference is substantially greater and more consistent in March. The reason for the difference is clear from Fig. 11, which is an equidistant azimuthal map centered on Giglio Island, Italy, showing the major thunderstorm centers of the world (as given in Ref. 18). The relatively close central Africa thunderstorm region is directly south of Italy, yielding a substantial contribution to the spectral noise density at 3 kHz in both March and June. To the east and west are also located two major thunderstorm regions, but they are significantly more distant and presumably produce a lower contribution to the spectral noise density. However, as Fig. 11 shows, during the summer the number and area of thunderstorm centers increase substantially for regions to the east and west of Italy but not for regions to the north and south. The June measurements reflect this change in thunderstorm-region distribution; the north-south and east-west noise levels are frequently comparable, particularly in the late afternoon and at night. During the morning minimum, however, the east-west noise is usually lower than the north-south noise.

A comparison of the March and June data taken in Italy shows that a noteworthy difference is the slow afternoon increase in noise starting at about 1100 UT in June. This noise increase may result from the summertime increase in afternoon thunderstorm activity around the world and may not be related to any change in propagation conditions. Our APD

16
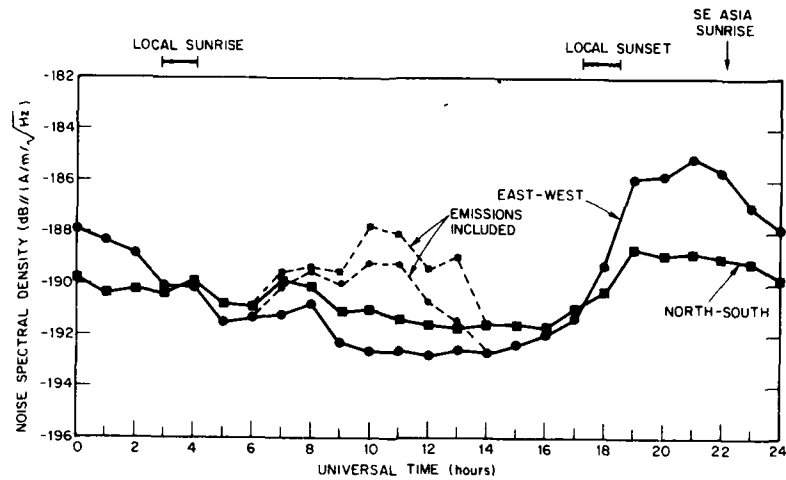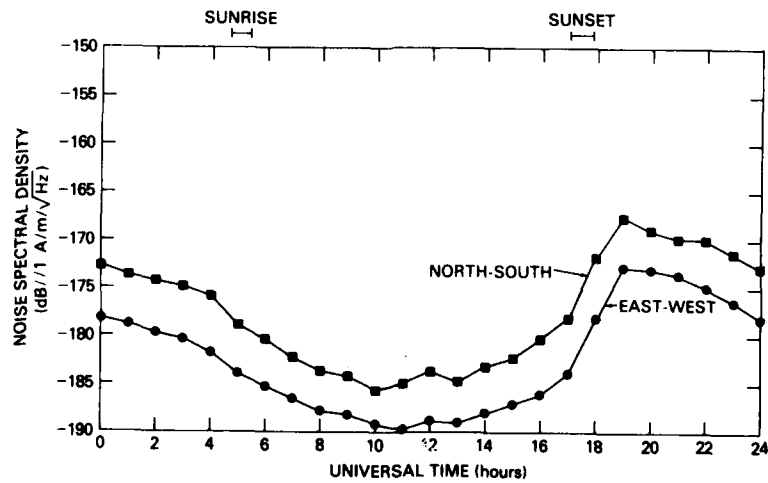
(a) Norway
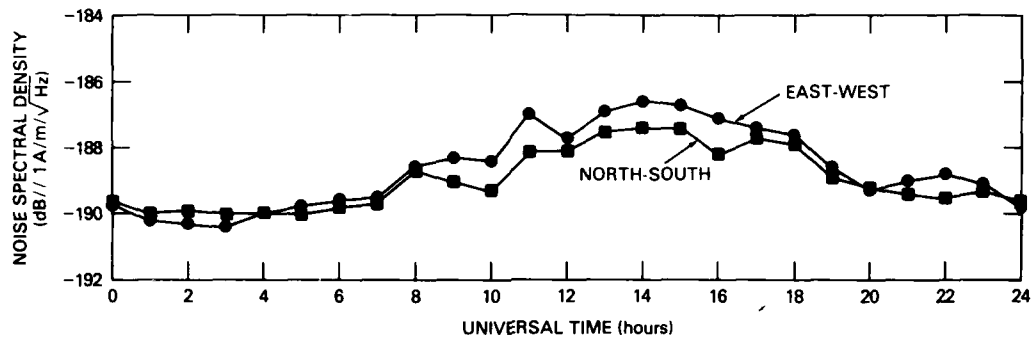

(b) Italy
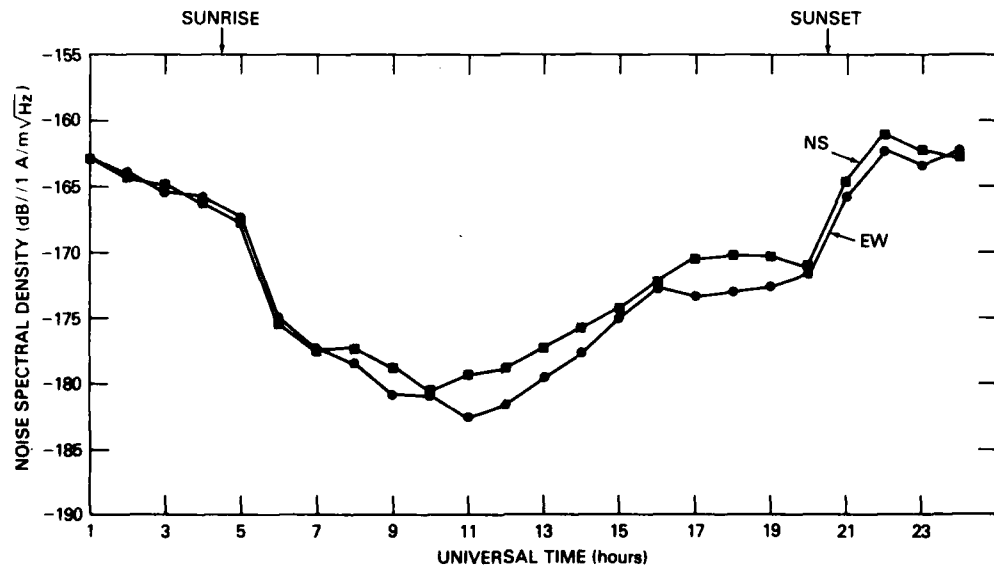
Fig. 9 — Average diurnal variations of the noise spectral density
at 3 kHz in March and April 1978

17

(a) Norway

(b) Italy

Fig. 10 — Average diurnal variation of the noise spectral density at 3 kHz in June 1978
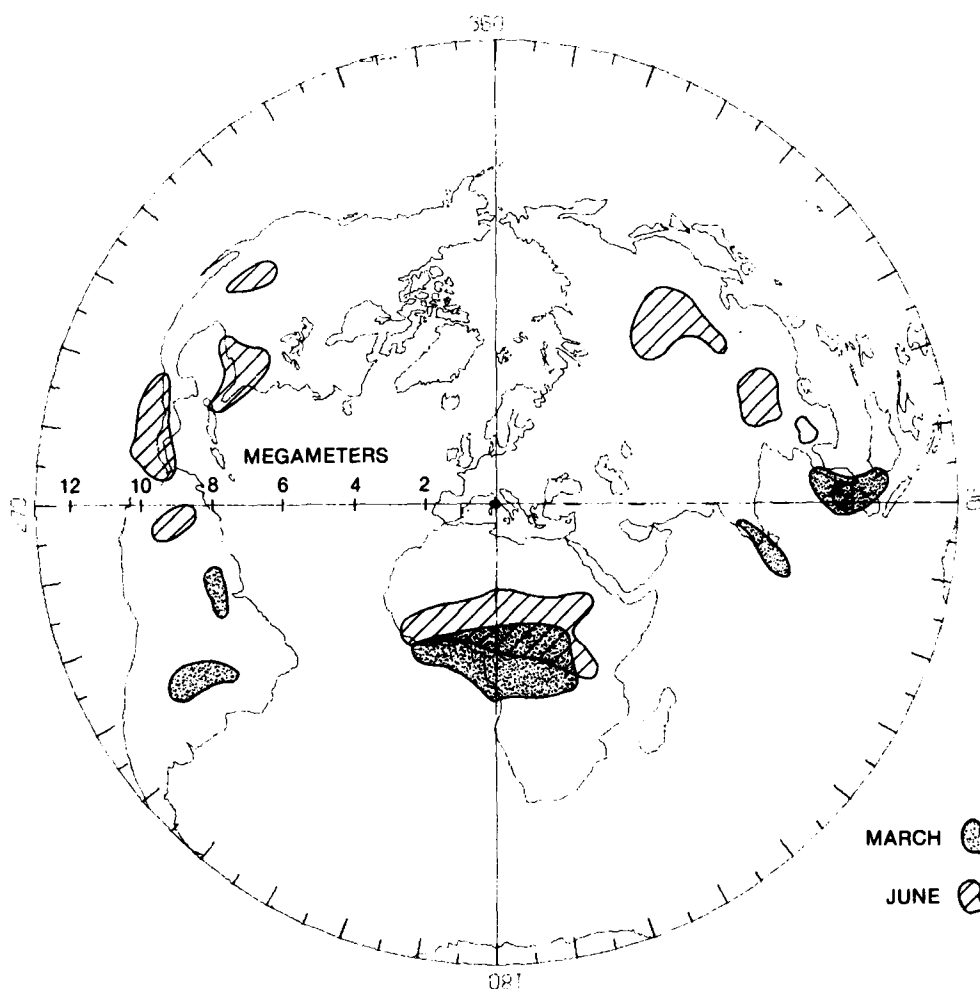
Fig. 11 — Equidistant azimuthal map centered on Giglio Island, Italy, showing major thunderstorm regions. Contours of 10 or more thunderstorms per month, taken from Ref. 18, are given for March and June.

measurements support this interpretation as follows. In the next main section we will discuss models of atmospheric noise that separate the noise into two components: a non-Gaussian impulsive component resulting either from nearby thunderstorms or from enhanced propagation conditions (as at night) and a Gaussian-distributed "background" component that is the superposition of many distant impulses. We will show in the next main section by comparing our measured APDs with an atmospheric noise model that our data are consistent with an increase in noise during the afternoon due to an increase in the Gaussian background component alone and not in the impulsive component.

Local Meteorological Influences

The general shape of the diurnal variation has been interpreted in terms of spatial and temporal variations in both the noise source (distant thunderstorms) and the intervening propagation channel (the earth-ionosphere waveguide). However, a number of significant deviations from the average diurnal variation are noticeable in Figs. 5 through 7. By examination of the recorded spectra during the periods of noise enhancement, their origin can be attributed to two causes: ionospheric emissions (observed only in Norway) and abnormally high atmospheric impulses from thunderstorms. The ionospheric emission events will be discussed in a later section; here the abnormally high atmospheric impulses are correlated with *local* storms (less than 1 Mm away).

In Italy abnormally high noise occurred on 18 and 24 March (Fig. 6). On both days the usual daytime minimum was not observed, and the noise remained near its high nighttime level throughout the day. Synoptic meteorological charts for Europe were obtained from the Naval Weather Service Detachment, Asheville, North Carolina. These charts, which plot conditions at 6-hour intervals, show that on both 18 March and 24 March an intense cold front moved across southern Europe and the Mediterranean with widespread thunderstorm activity. No thunderstorm activity was observed at or near the Giglio Island recording site on either day; however, the synoptic charts showed thunderstorm activity within 150 km.

In Norway the June 1977 data (Fig. 5) show two periods of high noise levels on 15 and 19 June that are not related to any ionospheric emission event. These high noise levels were caused by thunderstorms within a 200-km range spawned by a polar cold front that moved across northern Norway on these days. Nonlinear noise processing during these periods will be discussed in a later section.

Several other less obvious peaks in the Norway noise can probably be attributed to specific thunderstorm activity. On 27 and 29 June in the 1978 Norway data (Fig. 7) a midday peaking of the noise is evident that can be attributed to thunderstorm activity in southern Norway.

Enhanced East-West Propagation

The March 1978 data taken in Norway produced a surprising and unexpected result. Figure 6 and the averaged diurnal variation in Fig. 9 show that following local sunset the east-west noise spectral density quickly rises above the north-south noise density and at 2100 UT exceeds the north-south noise density by 4 dB. The difference consistently occurs. Appendix B is a discussion of the statistical significance of the difference, where it is shown that the difference is significant at the 10^{-4}% level. The east-west noise then falls slowly through the remainder of the night until the east-west and north-south noise densities become approximately equal at 0400 UT. During the daytime the east-west noise is usually 1 to 1.5 dB *less* than the north-south noise. The surprising result is the sharp increase in the east-west noise spectral density at sundown and its high value compared to the north-south noise. Figure 12 is an equidistant azimuthal projection map centered on Tromsø, Norway, showing the major thunderstorm centers of the world. The distance from Norway to the equatorial African sources to which the north-south loop is most sensitive is about 7 Mm,
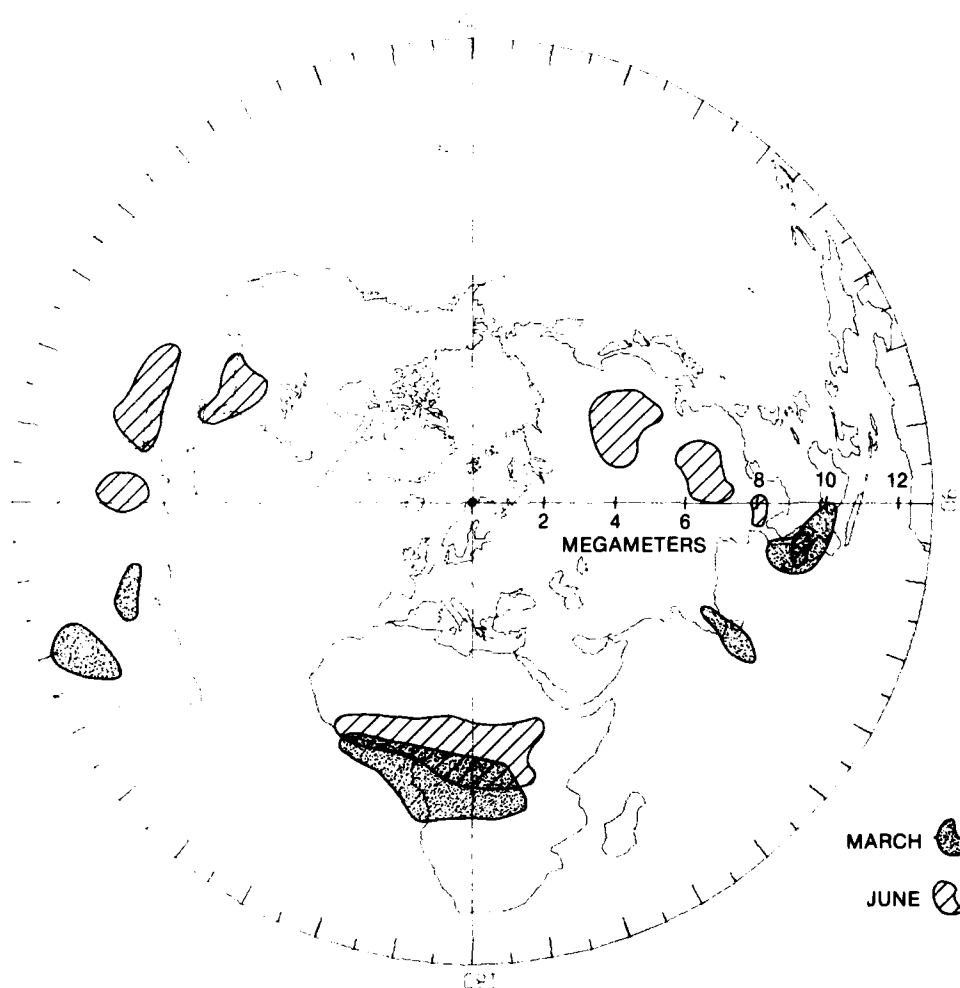
Fig. 12 — Equidistant azimuthal map centered on Tromsø, Norway, showing major thunderstorm regions. Contours of 10 or more thunderstorms per month, taken from Ref. 18, are given for March and June.

and the distance to the southeast Asian sources to which the east-west loop is most sensitive is about 10 Mm. If both regions have the same noise-density source strength on the average, the north-south noise would be expected to have the higher noise spectral density on the basis of the smaller source distance.

That the increased east-west noise is caused by thunderstorm activity in the Southeast Asia area can be shown by the following arguments. First, consider Fig. 13, which shows two typical examples of a direction-finding analysis performed on the north-south and east-
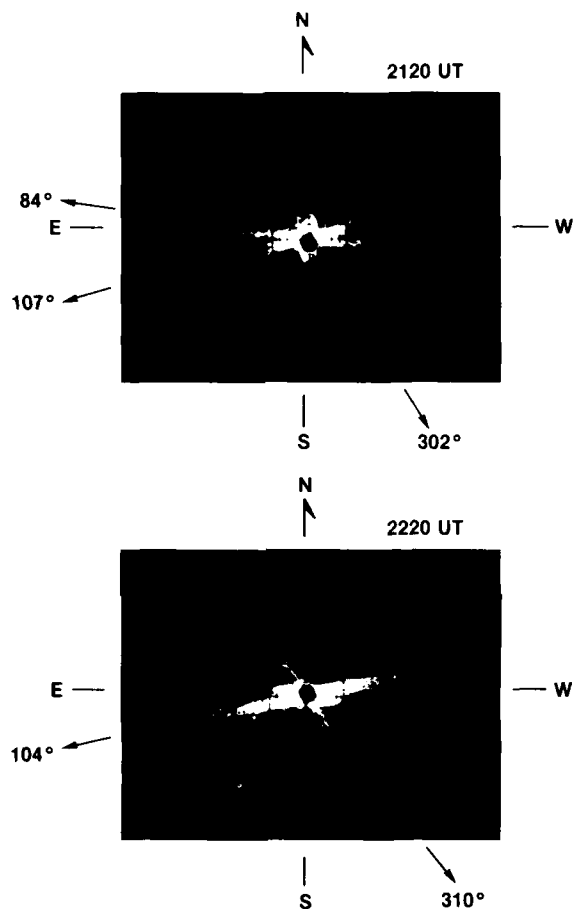
Fig. 13 — Polarizaton of atmospheric noise as recorded in
Norway (23 March 1979, 20-s interval). East and west are
shown reversed from their usual orientation because of the
polarity of the inputs to the oscilloscope.

west data, in the manner described in the preceding main section. The bearings for the top
photograph indicate a source at 302° in Africa (Fig. 12) but indicate two sources producing
somewhat stronger impulses at 84° and 107° in Asia. The bottom photograph shows the
much higher signals in the direction of the Asian sources; this photograph indicates that
both the impulsive component and the Gaussian background component display a clear
orientation toward the Asian source. Almost all of our other direction-finding photographs
taken after sunset produced results similar to the photographs in Fig. 13. As a second indica-
tion that the enhanced east-west nighttime noise results directly from Asian thunderstorm
sources, the time at which sunrise occurs near the Southeast Asian thunderstorm center is
indicated on Fig. 9 at about 2230 UT. The east-west noise is observed to drop noticeably

at that point. The east-west noise then continues to decrease slowly until sunrise over the measurement site for two reasons: the mixed night-day path between Southeast Asia and Norway gradually contains a higher percentage of daylight, with its higher attenuation rate, and the normal diurnal variation of thunderstorm occurrence has a minimum in the local morning hours at the thunderstorm location.

We hypothesize that the predominance of nighttime east-west noise over north-south noise, in spite of the significantly closer range of the thunderstorm sources in the north-south direction, is caused by a large anisotropy in the 3-kHz attenuation coefficients; that is, the average attenuation coefficient over the path from Southeast Asia to Norway is significantly lower than the coefficient over the path from Africa to Norway. The factors that can cause an anisotropy in ELF and VLF signal attenuation are known [16] to include the angle between the direction of propagation and the earth's magnetic field, cosmic-ray intensity (whose resulting ionizing influence is greatest near the geomagnetic poles), D-region winds, and ground conductivity.

We believe that essentially all of the lower attenuation rate over the east-west path arises from a more favorable angle of propagation of the noise impulses with respect to the earth's magnetic field. The consistency of the east-west noise dominance over the north-south noise eliminates such highly variable effects as cosmic-ray ionization and D-region winds as the probable cause, and the ground conductivities over the east-west Asia-to-Norway and north-south Africa-to-Norway paths are similar, since no large expanses of ocean are involved in either path. Theoretical support for the hypothesis that the propagation angle relative to the earth's magnetic field causes the enhanced east-west noise is provided by the theoretical calculations of Barr [1,19]. His curves of attenuation coefficient versus frequency, taken from Ref. 19 and shown in Fig. A1 in Appendix A, clearly indicate that near 3 kHz the attenuation coefficient for east-to-west propagation is about 16 dB/Mm less than north-south propagation. Additional curves computed by Barr in Ref. 1 show even larger anisotropies. We emphasize that Barr's calculations used a *daytime* ionospheric model (Deeks [20]) and hence cannot be compared directly with our nighttime data. To our knowledge attenuation-coefficient computations for a nighttime ionosphere have not been reported in the literature for frequencies within the attenuation band. However, although the specific values of the attenuation coefficients would be substantially smaller as the result of a computation that uses a nighttime ionospheric model, we believe that the relative difference in the coefficients for east-to-west and north-south propagation would still be similar to Barr's daytime calculations.

It would clearly be of interest to calculate the nighttime attenuation rates near 3 kHz using the methodology of Barr, but such a calculation was beyond the scope of the effort described in this report. In Appendix C we discuss how approximate attenuation rates could be derived from our experimental noise data for comparison with a (future) theoretical computation of attenuation rates.

Comparison of Our Spectral Noise Densities with Those of Other Investigators

Most of the measurements we referred to in the section reviewing previous work used electric-field antennas (usually a vertical whip), which yield measurements of the electric field. One might attempt to convert these electric-field values to equivalent magnetic-field values for comparison by dividing by the free-space wave impedance of 377 ohms. However,

this procedure is not valid near 3 kHz, because the earth-ionosphere waveguide modifies the wave impedance to a nonnegligible degree near the waveguide cutoff frequency. Hence, we cannot compare our magnetic-field intensity values with the many reported electric-field intensity values. In addition, as we mentioned in the earlier section, many of these early measurements appear to be contaminated by man-made noise.

In Fig. 14 we compare our spectral noise densities with those of two other investigators who used loop antennas to measure the magnetic field directly. Our values are on the average substantially lower. The value from Heirtzler et al. [7] is a single spot value. Feltham's spring value [13] was taken from one day of data that may represent an abnormally noisy day. The summer value is an average of several days of data. Although the data points chosen for comparison may not represent noise measured under similar conditions, we feel that Fig. 14 emphasizes the need for a carefully designed receiver and a quiet location in order to avoid contamination by man-made noise.
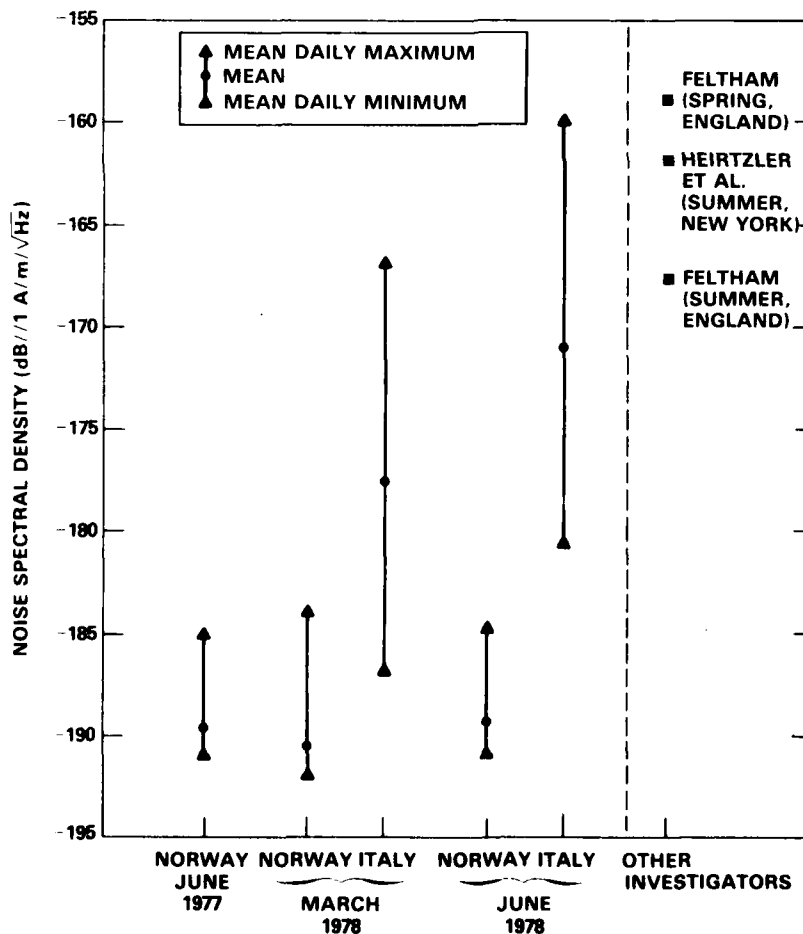

Fig. 14 — Comparison of the noise spectral densities at 3 kHz measured in this work with noise spectral densities at 3 kHz measured by other investigators

24

AMPLITUDE PROBABILITY DISTRIBUTIONS AND COMPARISON WITH NOISE MODELS

Measured APDs

Typical APDs measured in Norway and Italy are shown in Figs. 15 and 16 respectively. The abscissa indicates the percentage of time (during the 2-minute measurement interval) that the noise amplitude on the ordinate scale is exceeded. All of the APDs in this report are plotted as the log of the magnetic-field strength versus log-log of exceedence, a presentation commonly known as a Rayleigh probability plot. On this plot the band-limited envelope of a noise voltage composed of Gaussian-distributed quadrature components will be a straight line of slope −1/2; hence deviations from this straight line readily reveal non-Rayleigh (or complex Guassian) noise components.

In Fig. 15 the APDs from 23 March at 1300 UT and 21 June at 1500 UT represent low atmospheric noise and high atmospheric noise respectively as measured at the Norway site.
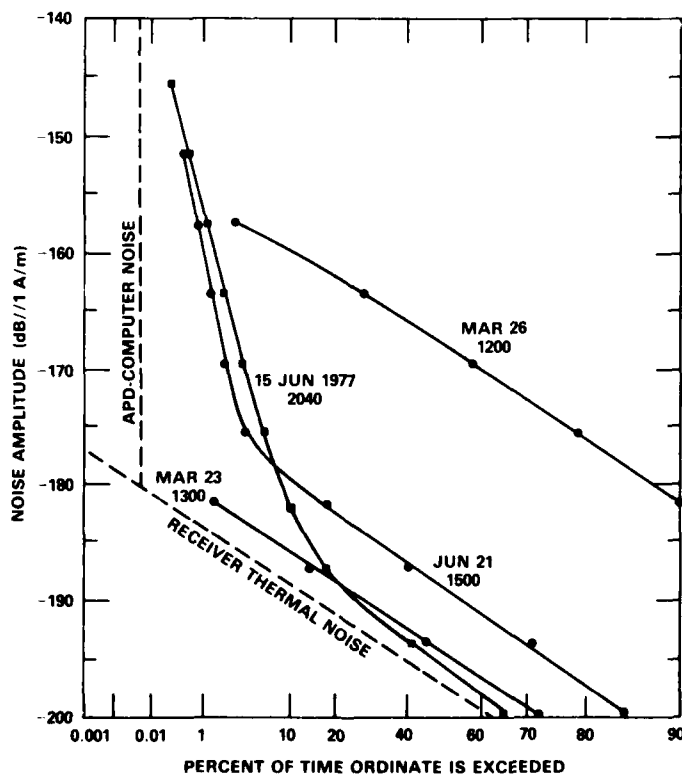

Fig. 15 — APDs measured in Norway (north-south antenna, 150-Hz noise bandwidth)
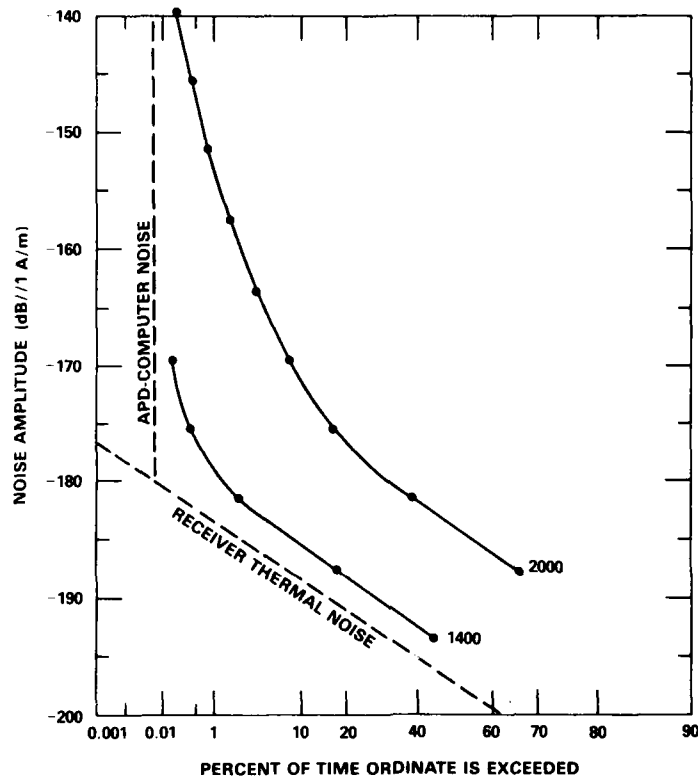
25

Fig. 16 — APDs measured in Italy on 15 June 1978
(north-south antenna, 150-Hz noise bandwidth)

The 21 June example shows the tail at low exceedence values that is characteristic of impulsive noise. The impulsive portion of the noise was caused in this case by a thunderstorm centered over southern Norway. The APD from 15 June 1977 at 2040 UT was measured during a local thunderstorm (one of only two local storms that occurred during our Norway measurements). This APD is noteworthy for its long tail, due to the thunderstorm, in combination with a particularly low value of the Gaussian component (At high exceedence values the APD is nearly depressed to the level set by receiver thermal noise.) Finally in Fig. 15 an APD is shown from 26 March 1978 that was recorded during an ionospheric emission event (These emissions are discussed in a later section.) The emissions, in the 150-Hz noise bandwidth of the receiver, have a Rayleigh distribution after envelope detection and are sufficiently large in amplitude to mask any atmospheric noise impulses.

Two examples of APDs recorded in Italy are shown in Fig. 16 and are typical of APDs recorded during high and low noise. The APDs recorded in Italy during low noise almost always had at least a small low exceedence tail, as shown in Fig. 16; by comparison the

Norway APD during low noise usually did not deviate from a straight line, as shown in Fig. 15. APDs during high noise in Italy displayed a gradual transition between the Rayleigh portion of the curve (at high exceedence values) and the tail at low exceedence values in comparison to the sharp knee in the Norway APDs. The transition in Italy is more gradual because the receiver is closer to the remote thunderstorm centers, giving rise to a larger spread in the amplitude and duration of received impulses. Thus the noise looks less like a two-component (Gaussian noise and impulsive noise) process.

Atmospheric Noise Models

A number of noise models exist in the literature for atmospheric ELF and VLF noise. We have limited our comparisons between the measured APDs and theory to two models: the Field-Lewenstein model [2] and the Middleton model [3].

The statistical nature of atmospheric noise can be characterized by a variety of functions in addition to the APD, including the probability density function, the crossing-rate distribution (number of positive crossings of a given voltage level, a function introduced by Rice [21]), and the distribution of the time interval between pulses [16]. However, the APD is the most convenient function to compare with experiment. In addition the APD can be used directly for the optimization of signaling formats, modem design, and other communication-system considerations.

Field-Lewenstein Model

The experimental APDs presented suggest two distinct components in VLF noise: one is approximately Gaussian, arising from distant storms whose impulses are relatively weak and unresolved, and accounts for the high-exceedence Rayleigh distribution in Figs. 15 and 16, and the other is an impulsive component, accounting for the tail, that presumably is from closer storms or particularly strong lightning flashes in distant storms. Field and Lewenstein [2] assume a "background" component represented by a Rayleigh density

$$\rho_1(x) = \frac{2x}{R_0^2} e^{-x^2/R_0^2}, \quad x \geqslant 0. \tag{3}$$

which has an average noise power $R_0^2 = 2\sigma_0^2$. The impulsive component is modeled to have a single-sided power-Rayleigh amplitude distribution:

$$\rho_2(y) = \frac{\alpha y^{\alpha-1} e^{-(y/R)^\alpha}}{R^\alpha}, \quad y \geqslant 0. \tag{4}$$

27

The parameter α takes on the values $0 \leqslant \alpha \leqslant 2.0$ and depends on the impulsiveness of the noise and on bandwidth. The smaller α becomes, the more impulsive the noise is. For $\alpha = 2$ the Rayleigh density in Eq. (3) results.

The composite probability density function $p(z)$ for the process $z = x + y$ is the convolution integral of Eqs. (3) and (4). Evaluating the probability density function and forming the APD according to the definition

$$\text{APD} = \text{Prob}\,(z > z_T) = \int_{z_T}^{\infty} p(z)\,dz \qquad (5)$$

yields the following expression for the APD:

$$\text{APD} = e^{-(z_T/R_0)^2} + \int_0^{z_T} \frac{2(z_T - z)}{R_0^2}\, e^{-(z/R)^\alpha - (z_T - z)^2/R_0^2}\,dz. \qquad (6)$$

This form of the APD was given by Field and Lewenstein in Ref. 22; it is somewhat different in form than the equivalent APD equation given by them in Ref. 2. Equation (6) yields an integral that is easier to evaluate on a computer than the equation in Ref. 2. To compare the experimental APDs with theory, the variance of $p(z)$ must be evaluated:

$$\sigma_z^2 = R^2 \left[\Gamma(1 + \frac{2}{\alpha}) - \Gamma^2(1 + \frac{1}{\alpha}) \right] + R_0^2(1 - \frac{\pi}{4}), \qquad (7)$$

where Γ is the gamma function. The substitution $z_T = \sigma_z \zeta_T$ is now made in Eq. (6); this substitution has the effect of referencing the APD variable z_T to the measured RMS level of the noise. The final equation for the Field-Lewenstein APD, in the most convenient form for comparison with the experimental APDs, is

$$\text{APD} = e^{-(\beta\delta\zeta_T)^2} + 2\delta\beta \int_0^{\zeta_T} (\zeta_T - \zeta)\, e^{-(\beta\zeta)^\alpha - (\delta\beta)^2 (\zeta_T - \zeta)^2}\,d\zeta, \qquad (8)$$

where $\delta = R/R_0$ and

$$\beta^2 = \Gamma(1 + \frac{2}{\alpha}) - \Gamma^2(1 + \frac{1}{\alpha}) + (1 - \frac{\pi}{4}) \frac{1}{\delta^2}\,.$$

The APD depends on only two dimensionless ratios: α and δ. The quantity δ can be cast in a form that is physically meaningful by calculating

$$\gamma^2 = \frac{E(y^2)}{E(x^2)} = \delta^2 \Gamma(1 + \frac{2}{\alpha}), \qquad (9)$$

where $E(...)$ refers to the expected value of the quantity in parentheses. Physically γ^2 is the ratio of the energy in the impulsive component to the energy in the Gaussian background component.

Equation (8) was fitted to the measured APDs by minimizing the total RMS error between the experimental exceedence values and the values given by Eq. (8). The values of α and γ producing the minimum error were determined by a two-level exhaustive search routine [23] searching a grid defined by $0 < \alpha \leqslant 2$ and $0.1 \leqslant \gamma \leqslant 12$.

In general we were able to obtain a good fit between our experimental APDs and the Field-Lewenstein model. Figure 17 is an example of a comparison with APDs recorded in Italy, showing in this case an excellent fit. Figure 18 compares an APD recorded in Norway with the Field-Lewenstein model; although the curve and the points do not match as well as in Fig. 17, the agreement can be considered good.

The fitting of the experimental APDs to the Field-Lewenstein model is time consuming and tedious, requiring hand entry of the exceedence values and nearly 10 minutes of computer time for each fitting determination. Therefore only portions of the data were selected
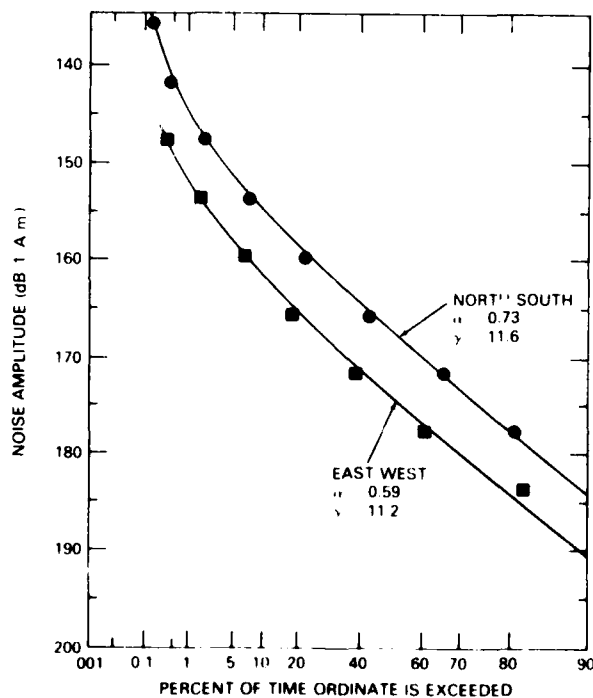

Fig. 17 — Comparison of APDs measured in Italy (19 June 1978, 2200 UT) with the Field-Lewenstein model of atmospheric noise
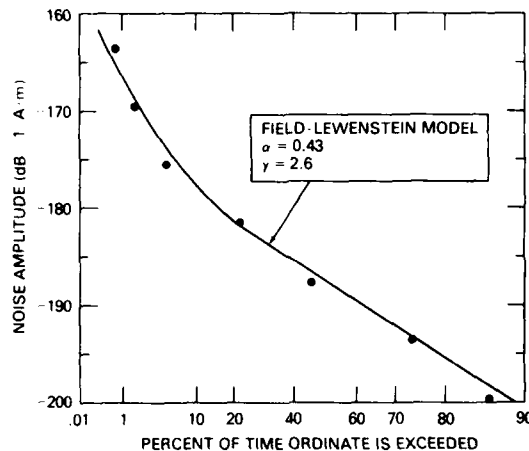
29

Fig. 18 — Comparison of APD measured in Norway (8 June 1978, 1600 UT) with the Field-Lewenstein model of atmospheric noise

for detailed comparison. For the Italian data, 26 June 1978 was chosen as a representative day, and hourly measured APDs were fitted to the Field-Lewenstein model. Figure 19 shows the result.

During the night, when the attenuation rate is lowest and the noise is the most impulsive, the value of γ is large, as expected. The fact that the variation in γ follows quite closely the variation in the RMS noise spectral density emphasizes that most of the noise power is concentrated in the impulses. One featue of the variation in the noise spectral density *not* followed by the variation in γ is the gradual increase in the noise through the afternoon; from 1200 to 1900 UT γ stays relatively constant, but the noise increases by nearly 5 dB. The implication is that the noise increase in this case is due as much to the increase in the background Gaussian component (arising from enhanced afternoon activity from distant thunderstorms, in this case probably in equatorial Africa) as to the increase in the impulsive component (from continental European sources). The parameter α in Fig. 19 remains relatively constant throughout the day, indicating that its particular value is determined predominantly by the specific receiver bandwidth and not by features of the noise.

Middleton Model

The Middleton [3] model of radio noise takes a more basic approach to developing an expression for such quantities as the probability density function and the APD than do other models such as the Field-Lewenstein model. The model starts by assuming a fairly general distribution of noise sources, emission waveforms, beam patterns, and propagation relations. The noise emissions as detected by a receiver are then summed statistically, and moments are calculated to determine the distribution. Because of its generality, the
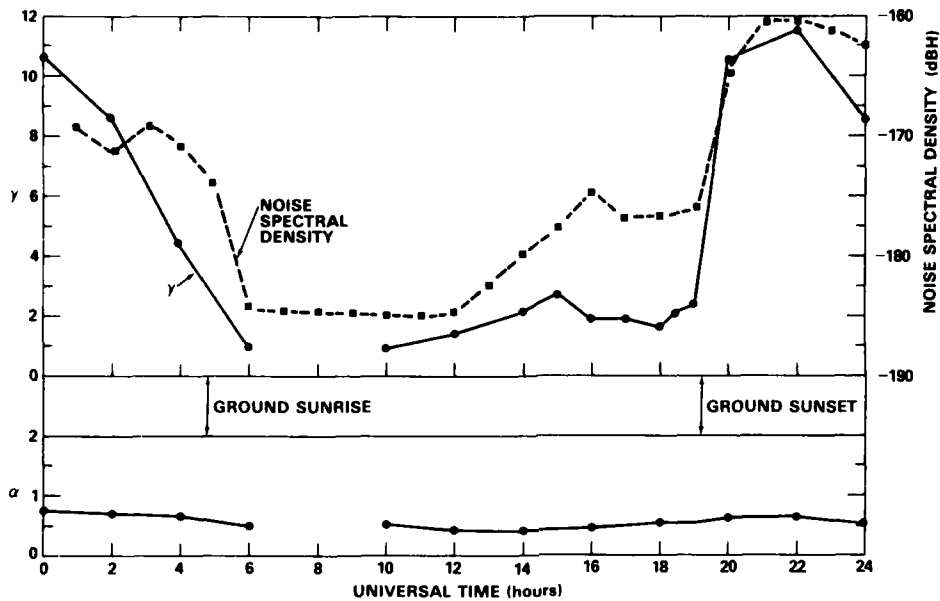
Fig. 19 — Variation of Field-Lewenstein-model parameters during
a typical day in Italy (26 June 1978, north-south loop)

Middleton model contains a large number of parameters (up to five), depending on the
class of noise considered. The Middleton formulation has been used in a wide variety of
radio-noise applications and has generally been successful in fitting experimental APDs [3].

In Middleton's taxonomy the noise here is class-B broadband noise. The derivation of
the relevant APD equation is quite lengthy, and here we only summarize the result.

To integrate some of the equations, Middleton finds it necessary to assume that the
radial variation of the source spatial distribution ξ is approximated by

$$\xi(R) \approx R^{-\mu}, \quad \mu > 0, \tag{10}$$

and that the propagation law from source to receiver follows

$$H(R) \approx R^{-m}, \quad m > 0. \tag{11}$$

Spherical spreading from a point source would require $m = 1$, and some waveguide modes
are approximated by $m = 0.5$. At 3 kHz the far-field propagation law actually follows an
equation of the form of Eq. (A7):

$$H(R) \approx \frac{e^{-\alpha R}}{\sqrt{\sin (d/a)}}. \tag{12}$$

31

Since Eq. (11) does not have this form, some problems with comparison of 3-kHz data with the Middleton model might be anticipated. We will discuss this point in more detail.

We will use a three-parameter version of the Middleton envelope APD for class-B noise:

$$\text{Prob} \, (z > z_T) = e^{-z_T^2/\Omega} \left[1 - \frac{z_T^2}{\Omega} \sum_{n=1}^{\infty} \frac{(-1)^n}{n!} A^n \, \Gamma(1 + \frac{\beta n}{2}) \right.$$

$$\left. \times {}_1F_1(1 - \frac{n\beta}{2} ; 2; \frac{z_T^2}{\Omega}) \right] , \tag{13}$$

in which Ω is a factor that normalizes the APD to the measured RMS noise level, Γ is the complete Gamma function, ${}_1F_1$ is a confluent hypergeometric function [24], A is an effective impulsive index related to the duration and number of source emission events, and β is a composite parameter related to the exponents μ and m defined in Eqs. (10) and (11) by

$$\beta = \frac{2 - \mu}{m} . \tag{14}$$

The parameter β must fall in the range $0 < \beta < 2$ to satisfy a constraint placed by the integration of Middleton's characteristic function [3]. The three fundamental parameters in Eq. (13) are Ω, A, and β.

We fit our experimental APDs to Eq. (13) by using a three-parameter sequential lattice search technique [23]. The comparison between the APDs and the Middleton model was usually satisfactory. Figure 20 shows a typical APD from Italy and the result of the best-fit Middleton model. The comparison, however, was not always as close as Fig. 20 indicates. In general we found that the low-exceedence-probability (high-amplitude) portion of the APD could always be fit well to the Middleton model, but the transition region and the high-exceedence-value portion sometimes differed by 2 to 3 dBA/m. We do not believe the difference is significant. Possibly the difference between Middleton's assumed propagation relation (Eq. (11)) and the actual evanescent form (Eq. (12)) that characterizes attenuation-band propagation accounts for the small lack of agreement under some circumstances. This hypothesis could be investigated by introducing the correct attenuation-band form at the appropriate points in the Middleton formulation. However, although we have not made an exhaustive study, it appears that the resulting integrals cannot be integrated in closed form. Numerical integration is of course always possible but was considered to be beyond the scope of the present study.
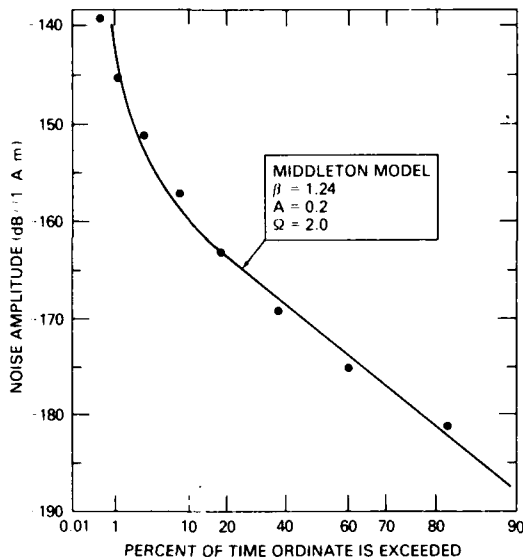
Fig. 20 — Comparison of an APD measured in Italy (19 June 1978, 2000 UT) with the Middleton model of atmospheric noise

For low exceedence values, so that $z_T^2/\Omega \gg 1$, it can be demonstrated, using the asymptotic development of $_1F_1$, that

$$\text{Prob}\,(z > z_T) \approx \frac{A\Gamma(1 + \frac{\beta}{2})}{\Gamma(1 - \frac{\beta}{2})} \left(\frac{\Omega}{z_T^2}\right)^{\beta} \tag{15}$$

This equation shows that, if the exceedence values are plotted on log-log paper vs z_T, then the points will fall on a straight line whose slope is -2β. Figure 21 shows the low exceedences from three selected APDs. The points in every case fall on a straight line, as predicted by the Middleton model. In general we found that if an APD has a well-defined low-exceedence tail, then the points on that tail (usually extending out to an exceedence of 5 to 15%) fall close to a straight line when plotted on log-log paper. The Middleton formulation agrees well with the high-impulse-amplitude, low-exceedence portion of the APD, and values for the physically interpretable parameter β can be derived.

Figure 22 shows the variation of β from midday on 19 June 1978 to the morning of 20 June 1978 in Italy. In general β shows a diurnal variation very similar to γ in the Field-Lewenstein model (Fig. 19); its value increases at sundown, corresponding to a steeper tail produced for the most part by enhanced propagation of distant atmospheric impulses. Interpreting the specific value of β is difficult, because by Eq. (14) the value depends on both a source parameter (μ) and a propagation parameter (m). Furthermore, the assumed propagation relation (Eq. (11)), as was pointed out, is of the wrong form to apply to the attenuation band. However, Eq. (14) does show that if we assume the source distribution is
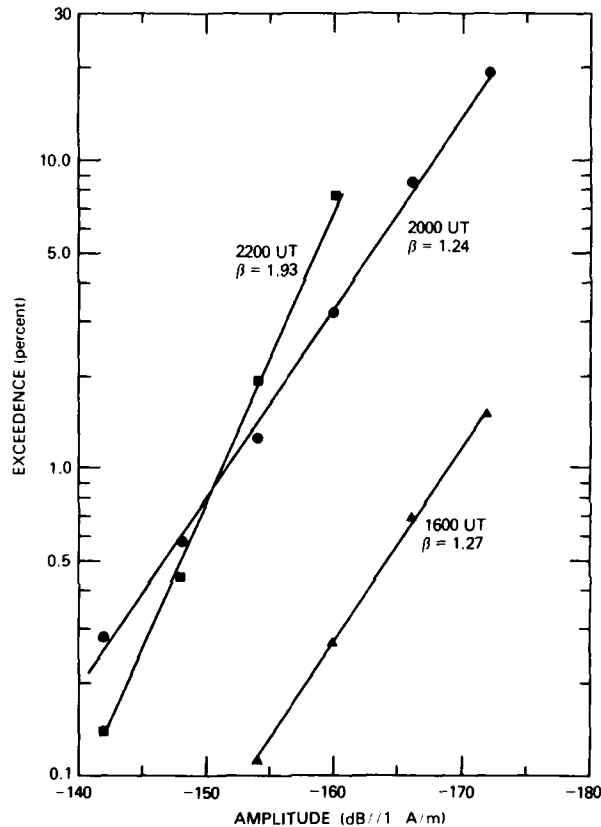
33

Fig. 21 — Logarithm of exceedence versus noise amplitude
for three typical APDs (measured in Italy, 21 June 1978,
north-south loop)

the same before and after sundown so that the source parameter μ does not change substantially, then the sharp increase in at sundown results from a decrease in m, corresponding to enhanced propagation.

One can examine a change attributable to a source variation by noting from Fig. 22 that β increases between 1100 and 1400 UT during the day, a period when the propagation conditions presumably do not change appreciably. Holding m constant in Eq. (14) shows that an increase in β implies a decrease in μ; by Eq. (10) a decrease in μ could reasonably be attributed to an enhanced contribution of nearby thunderstorms from continential Europe.

In short, although assigning a physical meaning to specific values of μ and m derived by comparing our measured APDs with the Middleton model is difficult, the functional dependance of the Middleton APD on those parameters agrees with the experimental data.
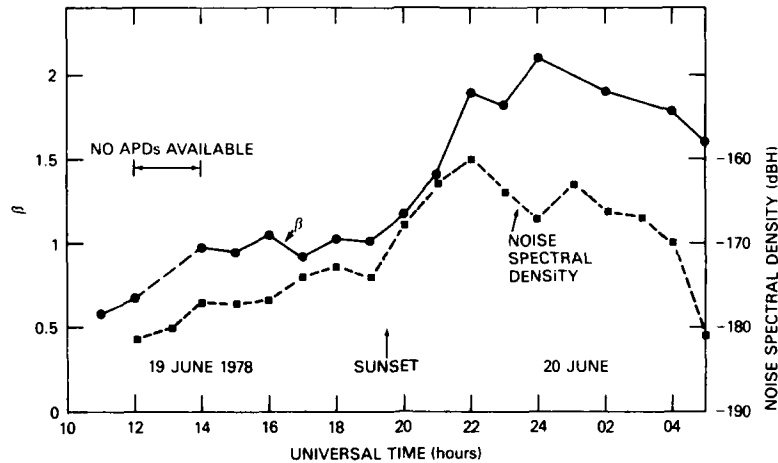
Fig. 22 — Variation of β in the Middleton noise model in Italy
(19 and 20 June 1978, north-south loop)

NOISE PROCESSING

The motivation for the present study of 3-kHz noise is the potential use of this frequency band for naval communications. In addition to investigating such features as the spectral, temporal, and source characteristics of the noise, we have also assessed the effect of using a simple nonlinear detector (a clipper) for reducing the effect of the ambient noise. This section describes the results of this noise processing.

It is well known that a nonlinear detector can improve the signal-to-noise ratio when one attempts to receive a small signal in non-Gaussian noise. Rappaport and Kurz [25] show that a nonlinear detector with an input-output characteristic given by

$$Y = \frac{d}{dx} \ln p(x), \tag{16}$$

where $p(x)$ is the probability density function of the noise, produces the optimal performance as long as the signal is quite small relative to the noise and as long as the samples of the noise are independent identically-distributed random variables. In the preceding section we presented measured APDs, from which we can derive a probability density function and, by Eq. (16), the shape of the optimal nonlinearity for 3-kHz noise. Figure 23 shows the probability density function and optimum nonlinearity $Y(x)$ deduced from a typical APD recorded in Italy in March 1978. For low amplitudes the output is proportional to the input, but for larger input amplitudes the transfer function bends over, and the output becomes inversely proportional to the input. Hence the optimum nonlinearity suppresses the large inputs arising from the atmospheric noise impulses. A similar shape for the optimum nonlinearity was derived for ELF noise by Evans and Griffiths [4].
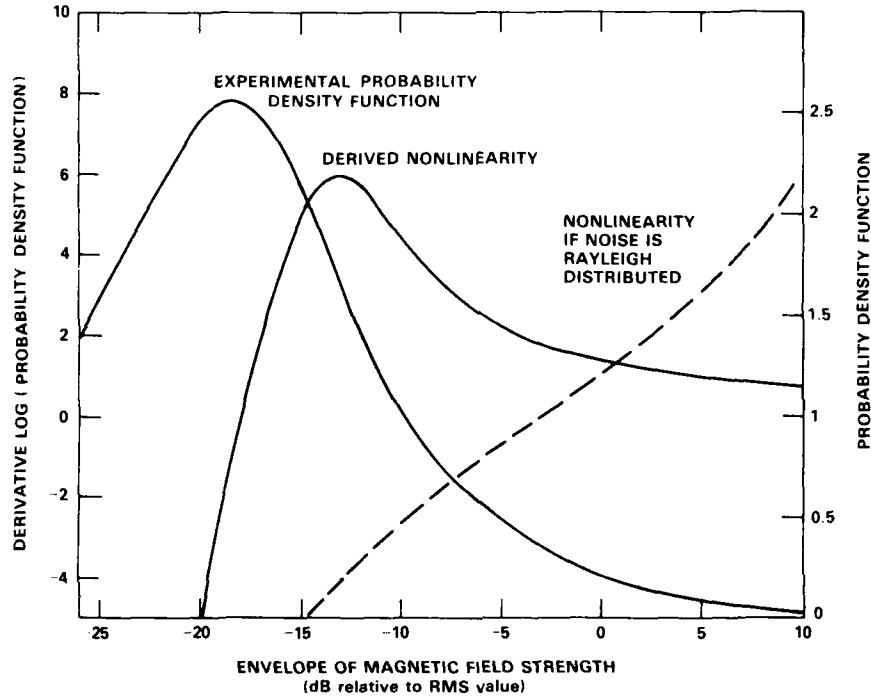
35

Fig. 23 — Probability density function derived from an experimental APD measured in Italy, the calculated optimum nonlinearity according to Eq. (16), and the detection law for Rayleigh-distributed noise (19 June 1978, 2200 UT, north-south loop)

The implementation of the nonlinearity shown in Fig. 23 in a practical receiver is difficult, and a nonlinearity that has the general shape and features of Fig. 23 but is easily constructed is required. Figure 24 shows three nonlinearities taken from Ref. 4 that are practical for a receiver. We have restricted our noise-processing investigations to the clipper transfer characteristic shown in Fig. 24, principally because results with ELF noise processing [4] have shown that the clipper consistently outperforms both the hole puncher and the hard limiter.

The goal of the clipper-processing study is to determine to what degree the effect of ambient noise on a 3-kHz receiver can be reduced. To this end we define an effective noise spectral level N_{eff} by

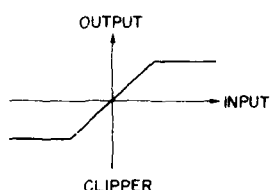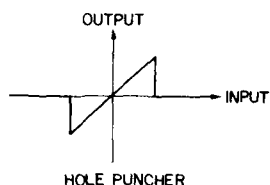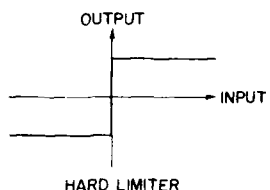$$N_{eff} = \frac{2H_s^2 \, T_m}{(SNR)_{NL}} = \frac{N_0}{I},$$

(17)

36

OUTPUT

INPUT

HOLE PUNCHER

OUTPUT

INPUT

Fig. 24 — Nonlinear detectors that can be implemented in a straightforward manner in a receiver

CLIPPER

OUTPUT

INPUT

HARD LIMITER

where $(SNR)_{NL}$ is the signal-to-noise ratio after clipping, H_s is the received signal H-field (in A/m), T_m is the matched filter integration time, N_0 is the raw spectral level of the ambient noise at the signal frequency, and I is the improvement factor using nonlinear processing. In other words, the nonlinear clipper processing is considered to produce a voltage at the output of a suitable matched filter (that follows the clipper) that is corrupted by *Gaussian* noise of spectral density N_{eff}.

Analysis Method

For most of the clipping investigations the outputs of the narrowband antennas were used, although the determination of the influence of bandwidth on N_{eff} used the output of the broadband antenna. The recorded noise was processed using a hybrid signal processor, in which the analog magnetic tapes were played back at several times the speed at which they were recorded through a parallel bank of multilevel clipping and filtering electronics. The filtered clipper outputs were then digitized, recorded on digital magnetic tape, and subjected to further processing by computer to compute effective noise levels and statistics.

The processor is essentially identical, except for an upward translation in frequency, to the processor described for similar ELF studies in Ref. 26. Figure 25 is a block diagram of the processor. The tapes were played back with a speedup factor of 2 through a parallel bank of four clippers. These clippers were adjusted to clip at levels from -146 dBA/m to -170 dBA/m in 6-dB increments. The clipped output was then filtered with a low-pass filter
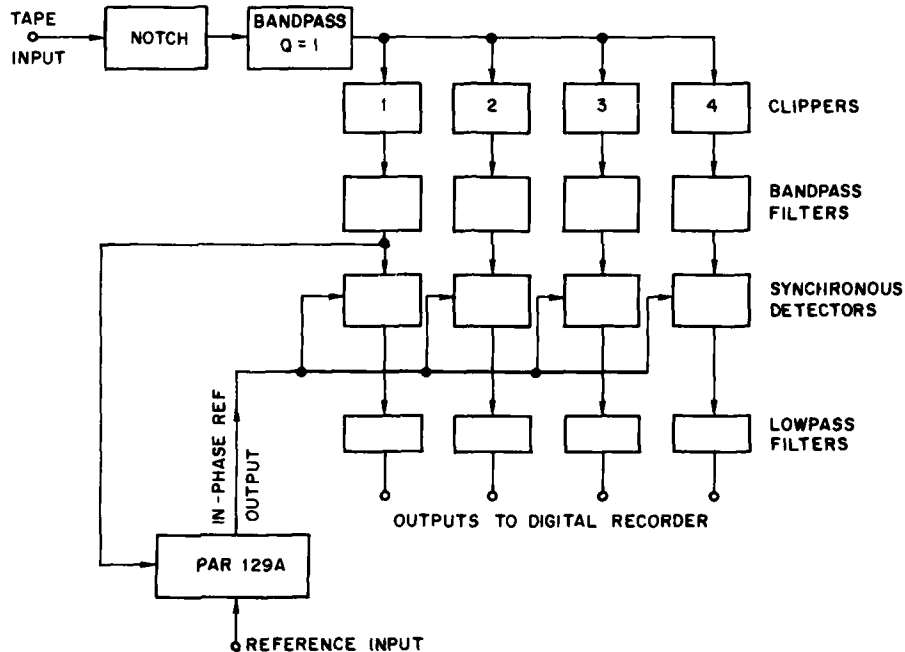
37

Fig. 25 — Clipping processor

to remove high-frequency components. One of the clipper outputs (in Fig. 25 the output of clipper 1 is shown) is applied to the signal input of a PAR model 129A lock-in amplifier operating in the vector mode. The low-level continuous calibration signal injected at the antenna output is thereby phased-locked to the reference signal that was recorded on a separate parallel tape channel. The output of the PAR 129A, which consists of a tone that is in phase with the low-level calibration signal, is then used as the reference for the four synchronous detectors. The output of each synchronous detector is the in-phase component of the low-level calibration signal corrupted by the clipped atmospheric noise. The four synchronous detector outputs are low-pass filtered with an effective real-time time constant of 1 second in order to yield a 1-Hz noise bandwidth. These outputs are digitized at a 50-Hz rate and recorded on digital tape.

The digital tape was processed on a digital computer; the effective noise was derived using Eq. (17) for each clipping level at an approximate interval of 10 minutes. At the completion of each analog tape (typically 16 hours of real-time data for Norway and 8 hours for Italy), the effective noise level, standard deviation, probability density, and cumulative probability distribution were computed.

Effect of Bandwidth

In planning for the more extensive June 1977 measurements in Norway and the two-site-coordinated measurements in 1978, the preliminary January 1977 data recorded in Norway on the wideband loop were analyzed to determine the influence of bandwidth on the effectiveness of the clipping. The object of the study was to establish the *minimum* bandwidth required for the tuned narrowband loops; that is, a compromise must be struck, since the lowest receiver intrinsic noise can be obtained by narrowing the bandwidth, but a bandwidth that is too narrow does not yield the best clipping performance, for the following reason. A clipper offers the biggest reduction in noise when large-amplitude impulses of short duration are present. However, narrowing the bandwidth prior to clipping has the effect of rounding off the impulses and distributing their noise power throughout the filter bandwidth, rendering the clipping less effective.

Figure 26 shows a typical result of the effect of bandwidth for data recorded on 13 January 1977. Two periods are shown: a relatively-low-noise period (1700 UT), when the spectral noise density was -178 dBH, and a high-noise period (2200 UT), when the spectral noise density was -171 dBH. Figure 26 demonstrates that as the bandwidth is increased, the effective noise decreases, as expected by the argument that was given; the influence of the bandwidth is slightly greater for the period of high noise, again an expected result, since the high-noise period in this case has more impulses that are adversely affected by narrowing the bandwidth. Figure 26 shows that only a marginal improvement results for a preclipping bandwidth greater than about 140 Hz. Based on these results, the narrowband loops used for the data taken in June 1977, March 1978, and June 1978 employed a noise bandwidth of 150 Hz.
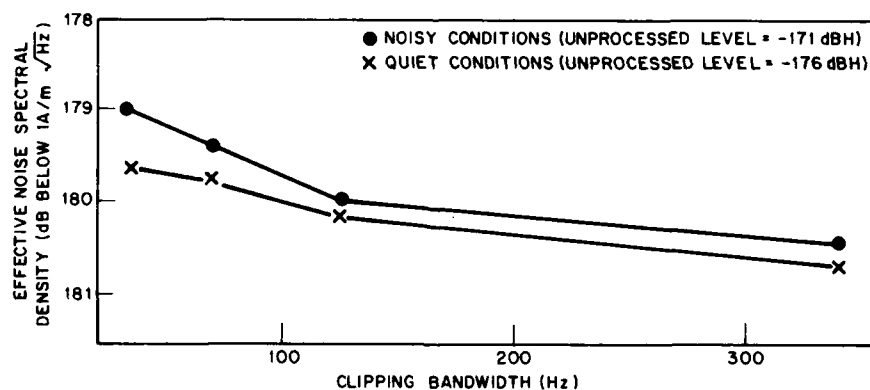
Fig. 26 — Influence of the clipping bandwidth on the effective noise

Italy Results

Figure 27 presents the average diurnal variation of the spectral noise density measured in Italy in both March and June 1978 (repeated from Figs. 9 and 10) and also shows the average diurnal variation of the effective noise N_{eff} for both measurement periods. For the

hourly averages the four values of N_{eff} produced by the four clipping levels were scanned, and the lowest value of N_{eff} was used in computing the average; in other words a constant clipping level was not used in constructing Fig. 27. The improvement (decrease) in the noise level due to clipping is seen to vary from 1 dB (noon in June) to a substantial 10.0 dB at 1900 in March. The overall average decrease in effective noise level is 6.7 dB for March and 3.3 dB for June. The smaller improvement in effective noise achieved in the June measurements is probably due to the enhanced thunderstorm activity in June both in equatorial Africa and over continental Europe. This activity (or, in the case of Europe, that portion of the activity beyond 1000 km or so) tends to increase the Gaussian "background" component of the noise relative to the local non-Gaussian noise component, rendering the clipping processing less effective.

In March, on the other hand, the average (unprocessed) noise level is lower, principally because the lower worldwide thunderstorm activity produces a lower Gaussian "background" component; but the intensity of the impulsive non-Gaussian component (arising from occasional local thunderstorms and intense flashes in distant storms) is still large. This circumstance leads to a larger improvement due to clipping in the March data than in the
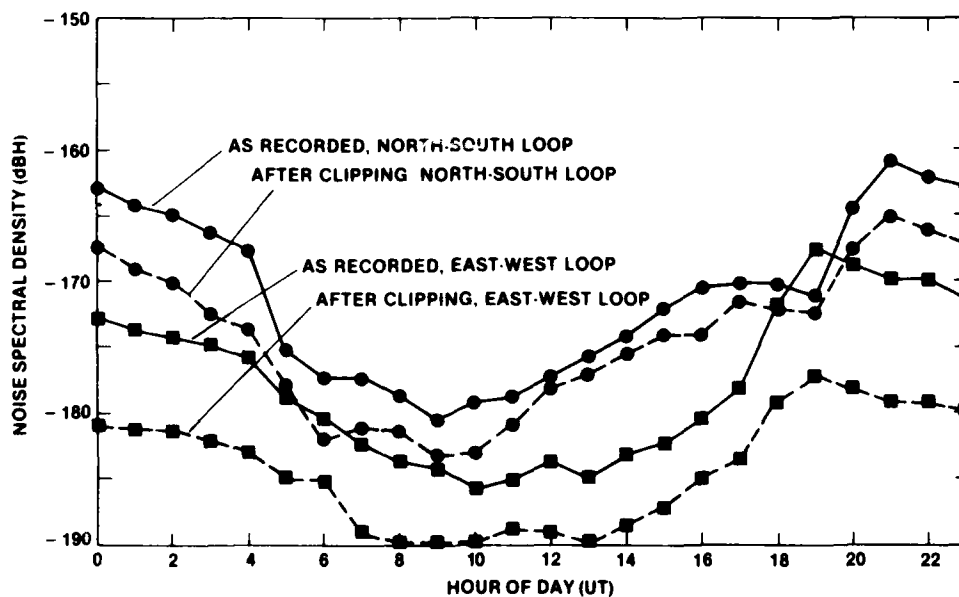

Fig. 27 — Average diurnal variation of the 3-kHz noise spectral density measured in Italy

June data. The noise in June also appears to have a larger proportion of many smaller impulses rather than a few large impulses, as compared with the March noise. Under these conditions the improvement due to clipping is expected to be smaller, since for many small impulses the clipper must operate a larger fraction of the time (during which the signal is turned off) to excise the same amount of noise power removed during the clipping of more infrequent large impulses.

In both March and June the processing improvement is substantially larger at night. The higher and more conductive ionospheric reflecting layer at night not only decreases the attenuation rate for the impulses but also produces less dispersion of the impulses; hence the impulses are larger and of shorter duration, both of which are factors that improve the effectiveness of clipping.

The effective noise level produced by clipping is relatively insensitive to the clipping level (within limits). Figure 28 shows the variations of the unprocessed spectral noise density and the effective noise density produced by three clipping levels on a day typical of the June data. During the more impulsive nighttime noise period the 12-dB spread in clipping level is observed to produce a variation of only 1 dB or less in effective noise. During the daytime noise period the specific clipping level has a somewhat larger effect, producing a variability of up to 3 dB in effective noise. From Fig. 28 it is evident that a clip level of -164 dBA/m most often produces the minimum effective noise level.
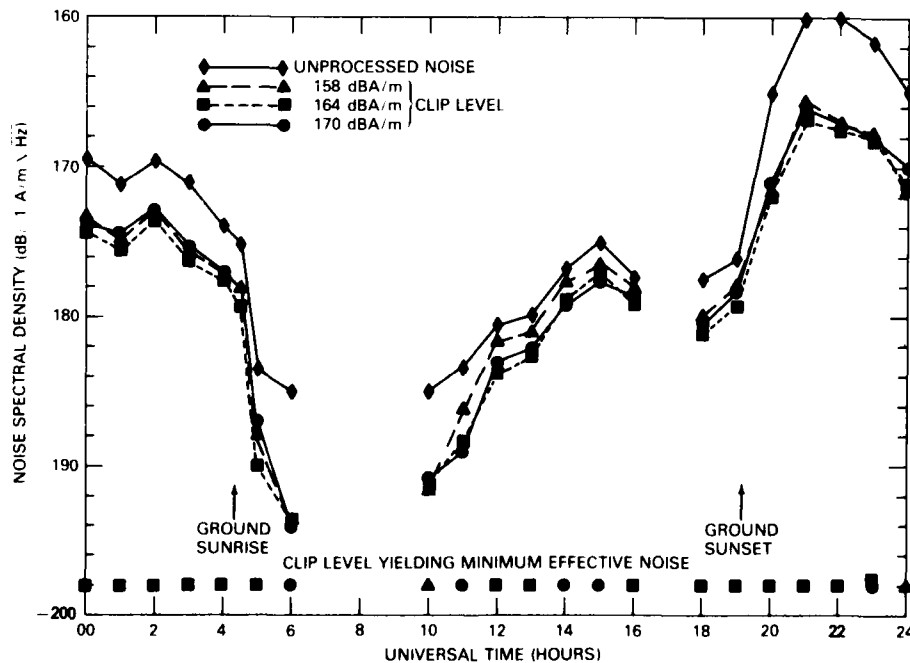

Fig. 28 — Unprocessed recorded noise spectral density in Italy (26 June 1978, north-south loop) and the effective noise after clipping at the indicated level

41

Norway Results

The discussions of the average diurnal variation and the APD showed that in northern Norway the noise spectral density is approximately Gaussian much of the time. Nonlinear processing, such as clipping, offers no reduction in noise spectral density when operating against Gaussian noise and in fact can increase the noise level if the clipping level is set too low in amplitude. Our clipping results on the Norway data confirmed this behavior and in general were erratic when the noise level decreased below about -188 dBH. Indeed, when the noise spectral density is already this low, there is probably little interest from a communication systems application in attempting to lower the noise any further by clipping anyway. Therefore we do not plot any comparison curves similar to Fig. 27 for the Norway data. Instead, we present several examples of the effect of clipping in Norway during periods of high noise.

The first example of a period of high noise level was recorded during one of only two verified occurrences of a local thunderstorm (range less than 500 km) observed during all of our Norway measurements. Figure 29 displays the noise spectral density and the effective noise level between 1600 UT on 15 June and 0800 UT on 16 June 1977. The high noise level resulted from a thunderstorm within an estimated 100 km of the Norway measurement site. At 2300 UT the thunderstorm dissipated rather abruptly, causing the noise level to
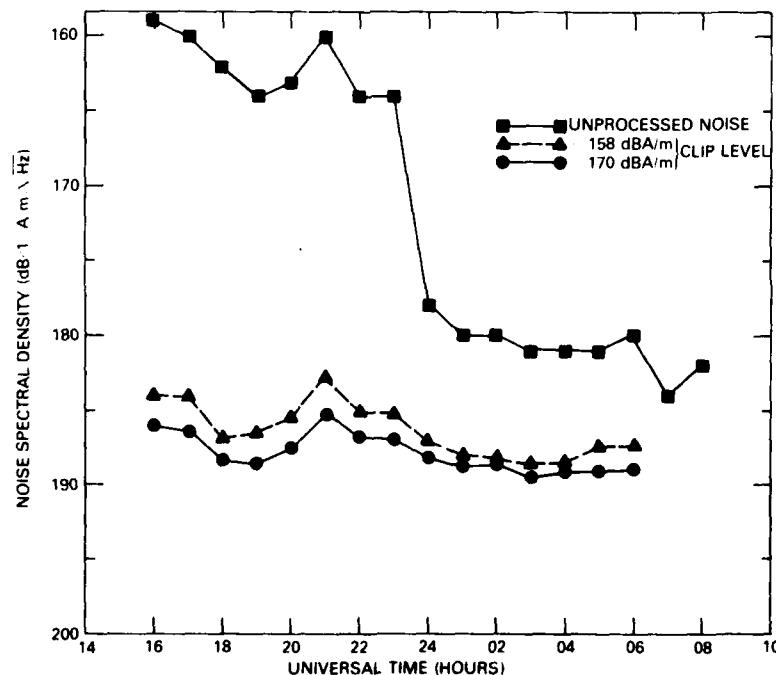

Fig. 29 — Effect of clipping during a period of a local thunderstorm in Norway
(15 and 16 June 1977, north south loop)

drop about 16 dB. Figure 15 contains an APD taken at 2040 UT during the storm showing a steep tail due to the nearby storm. The combination of an isolated thunderstorm cell producing large atmospheric impulses that are not broadened by having to propagate to a large range and a receiver located in an area where the background noise component is low in amplitude and very nearly Gaussian yields a large clipping improvement. At 1600 UT on 15 June a reduction of 26 dB is achieved; to our knowledge this reduction is higher than that achieved in any of the ELF studies [1,26,27] of noise excision by clipping. However, an improvement of this magnitude occurred only in this somewhat specialized case. A second thunderstorm occurred on 19 June 1977 that produced a noise spectral density (at the maximum activity of the storm) of -165 dBH (Fig. 5). Clipping during this storm lowered the effective noise spectral density to -184 dBH, an improvement of 19 dB.

As a second example of a high noise period in Norway, we consider the intense ionospheric polar chorus event observed on 26 March 1978. Figure 30 is a plot of the spectral noise density for 26 March 1978, showing the high noise spectral density from 0600 to 1400 UT resulting from the polar chorus emission. Also shown is the effective noise density achieved by clipping at a level of -170 dBA/m. In contrast to the improvement during a local thunderstorm, during the emission event the clipping produced at most only a 3-dB lowering of the effective noise. The nearly Gaussian character of the polar-chorus APD (Fig. 15) is not amenable to noise reduction by clipping, rs Fig. 30 illustrates.
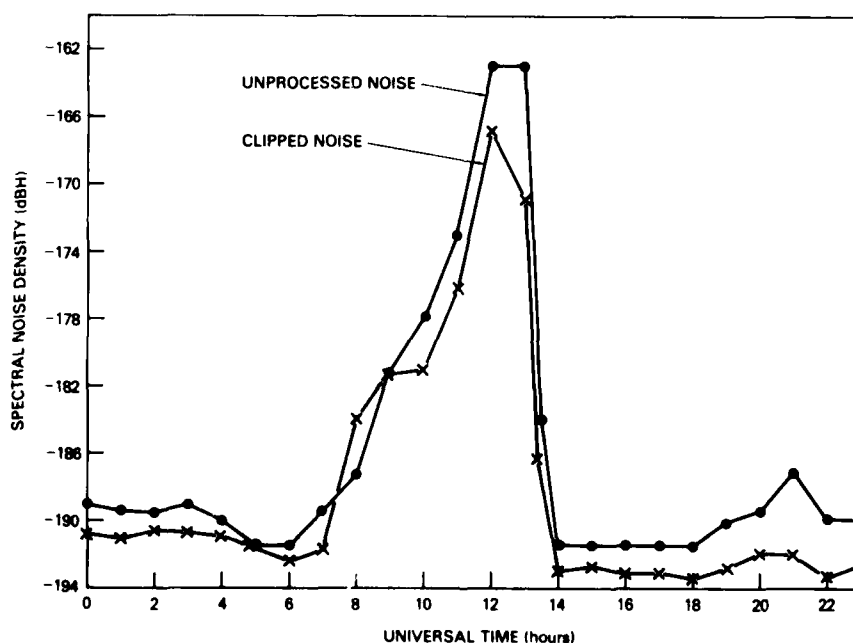

Fig. 30 — Effect of clipping during polar-chorus emissions in Norway (26 March 1978, north-south loop), showing only a small reduction in comparison with the reduction in Fig. 29

IONOSPHERIC EMISSIONS

We observed broadband emissions that were clearly of ionospheric or magnetospheric origin only at the Norway site. In Figs. 5, 6, and 7 we have indicated when broadband emissions were observed. Figure 31 is a time-spectral display of a particularly intense and lengthy emission event that occurred on 26 March 1978. Although this event is somewhat atypical, the spectral features shown in Fig. 31 were also observed in other emissions; specifically, Fig. 31 shows noise that is generally broadband, has no discrete frequency components, has a widely variable upper cutoff frequency, and has relatively little periodic structure. The emission event on 3 April 1978 is another instance of a long-lived event and was only slightly less intense than the event on 26 March 1978. The time-spectral display of this event is shown in Fig. 32. Both in this display and in Fig. 31 we have indicated the spectral interval over which the receiver response is essentially flat to emphasize two points: the sharp cutoff at low frequencies is a result of the receiver response, so that the emissions extend in an unknown manner to lower frequencies, and the variable upper frequency cutoff is not related to the receiver response, with the possible exception of the interval from 0800 to 0830 UT on 3 April 1978.

Comparison of Figs. 31 and 32 with the atlas of VLF emission spectra presented by Helliwell [14] indicates that these emissions are probably polar chorus, a term introduced
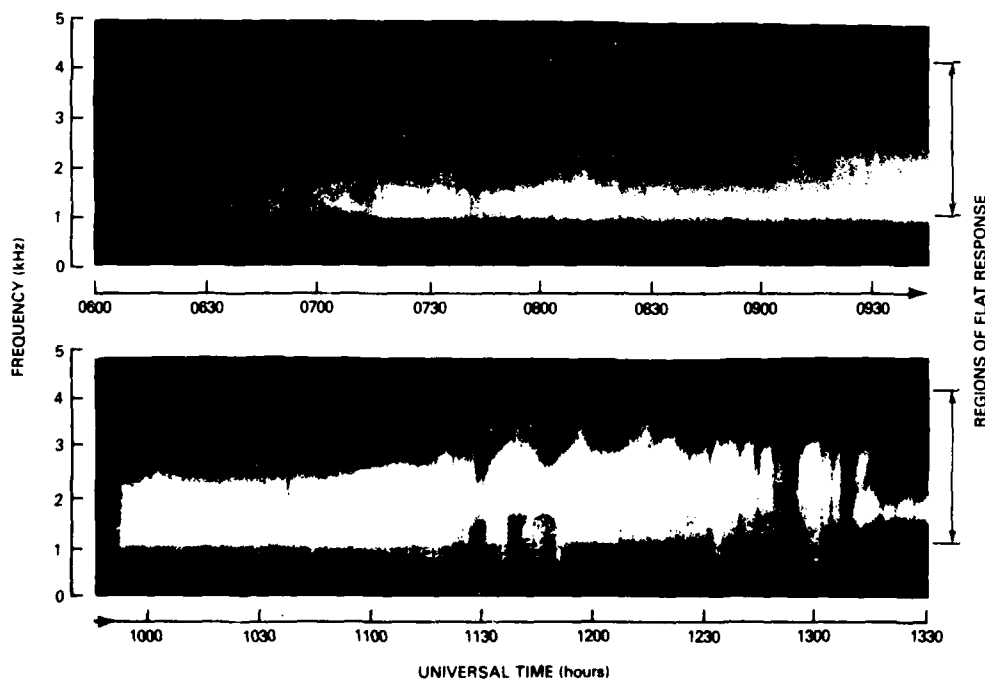

Fig. 31 — Time-spectral display of a polar-chorus emission event measured in Norway on 26 March 1978 (north-south loop). The emission onset occurred at approximately 0710 UT.
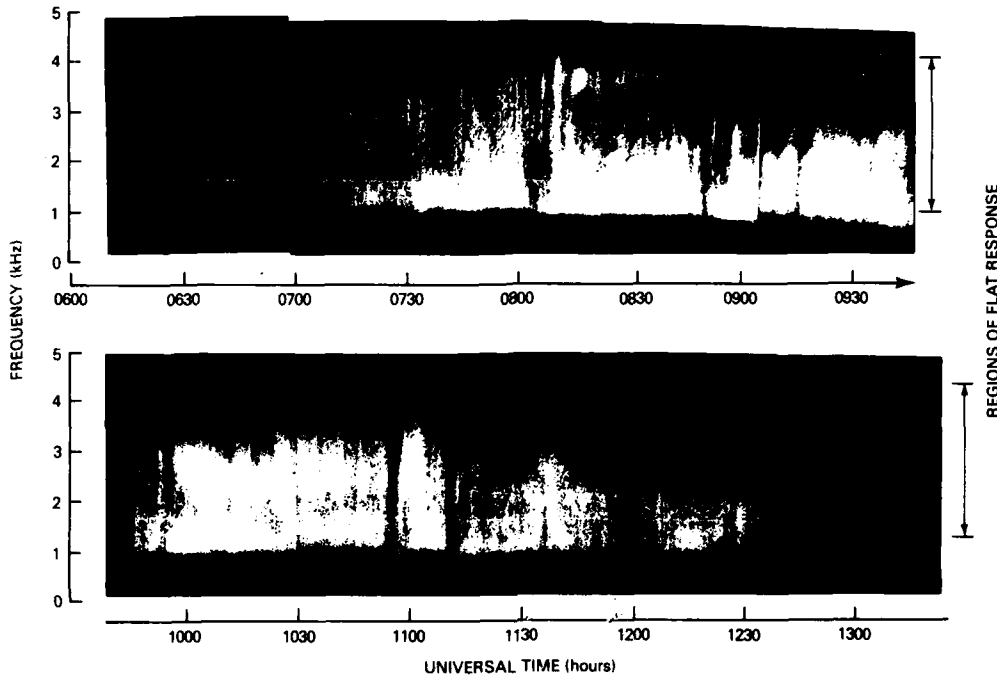
Fig. 32 — Time-spectral display of a polar-chorus emission event measured in Norway on 3 April 1٤ ‾8 (north-south loop). The emission onset occurred at approximately 0725 UT.

by Ungstrup and Jackerott [28]. A different class of emissions, auroral hiss, sometimes has an upper cutoff frequency near 3 kHz, but usually the cutoff is much higher. As further evidence that the emissions are polar chorus, Fig. 33 shows the diurnal variation of the emissions in Figs. 31 and 32 are polar chorus. and, for comparison, the diurnal variation of auroral hiss (as measured by Harang [29] in Norway) and polar chorus (as measured by Ungstrup and Jackeroff [28] in Greenland). The diurnal variation clearly suggests that the emissions in Figs. 31 and 32 are polar chorus.

Extensive analysis of the emissions is not warranted here because our data sample is somewhat limited. It is of interest, however, to investigate the time variation of the APD during the course of an emission event. Figure 34 displays the variation in the APD and the spectrum during the polar-chorus event on 26 March 1978. From 0000 to 0500 UT the spectra show a typical nighttime form, and the APDs have a well-defined low exceedence tail due to atmospheric noise impulses. At local sunrise (about 0500 UT) the spectra decrease in amplitude, the spectral minimum at 3 kHz is visible, and the APDs assume a straightline form indicative of Rayleigh noise, because daytime propagation conditions decrease the relative atmospheric impulse amplitude. At approximately 0700 UT the polar chorus begins; the APDs are observed to have a straightline Rayleigh form, but at a much higher RMS amplitude. Hence the polar-chorus emissions appear as intense broadband noise
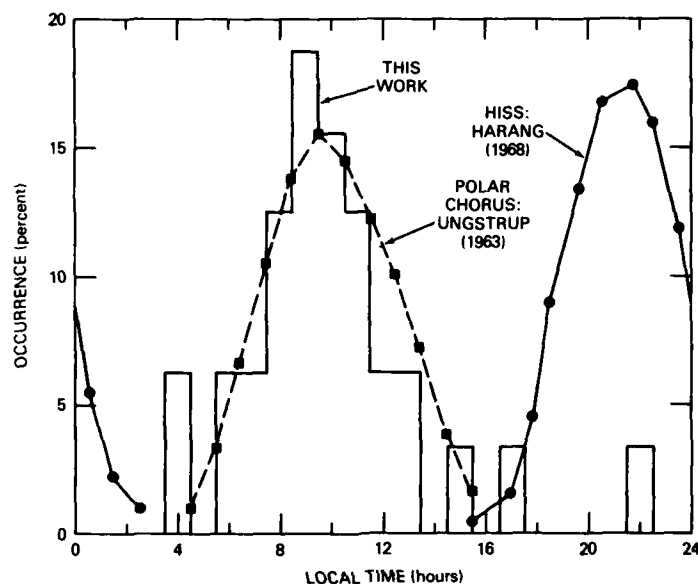
45

Fig. 33 — Diurnal variation of emissions observed during measurements in March and April 1978 compared with polar-chorus and hiss diurnal variations measured by other investigators

in the receiver bandwidth. Clipping of the noise during this period is fruitless, as was shown in Fig. 30. At about 1300 UT the event ends, and the APD and spectra assume their pre-event appearance.

Attempts were made to measure a direction of arrival for the noise using the simple direction-funding technique described in an earlier section, but the superimposed oscilloscope traces showed no clearly defined axis, either because the noise is nearly circularly polarized or because the source region is nearly over the measurement site.

The noise recorded in Italy was searched carefully at times of the emissions recorded in Norway, but no evidence of the emissions was ever observed in the Italy data.

VARIATION OF THE SPECTRAL MINIMUM

In Norway the minimum spectral noise density, corresponding to the frequency of maximum cutoff of modes in the earth-ionosphere waveguide, was nearly always well pronounced. In Fig. 34 the spectra always show a well-defined minimum, even during the polar-chorus disturbance. In Italy, on the other hand, a minimum in the spectral noise density was frequently not seen; instead the spectrum was often essentially flat across the response bandwidth of the broadband loop and receiver. The lack of well-defined minima in the Italy spectra probably results because the measurement site is relatively close to the
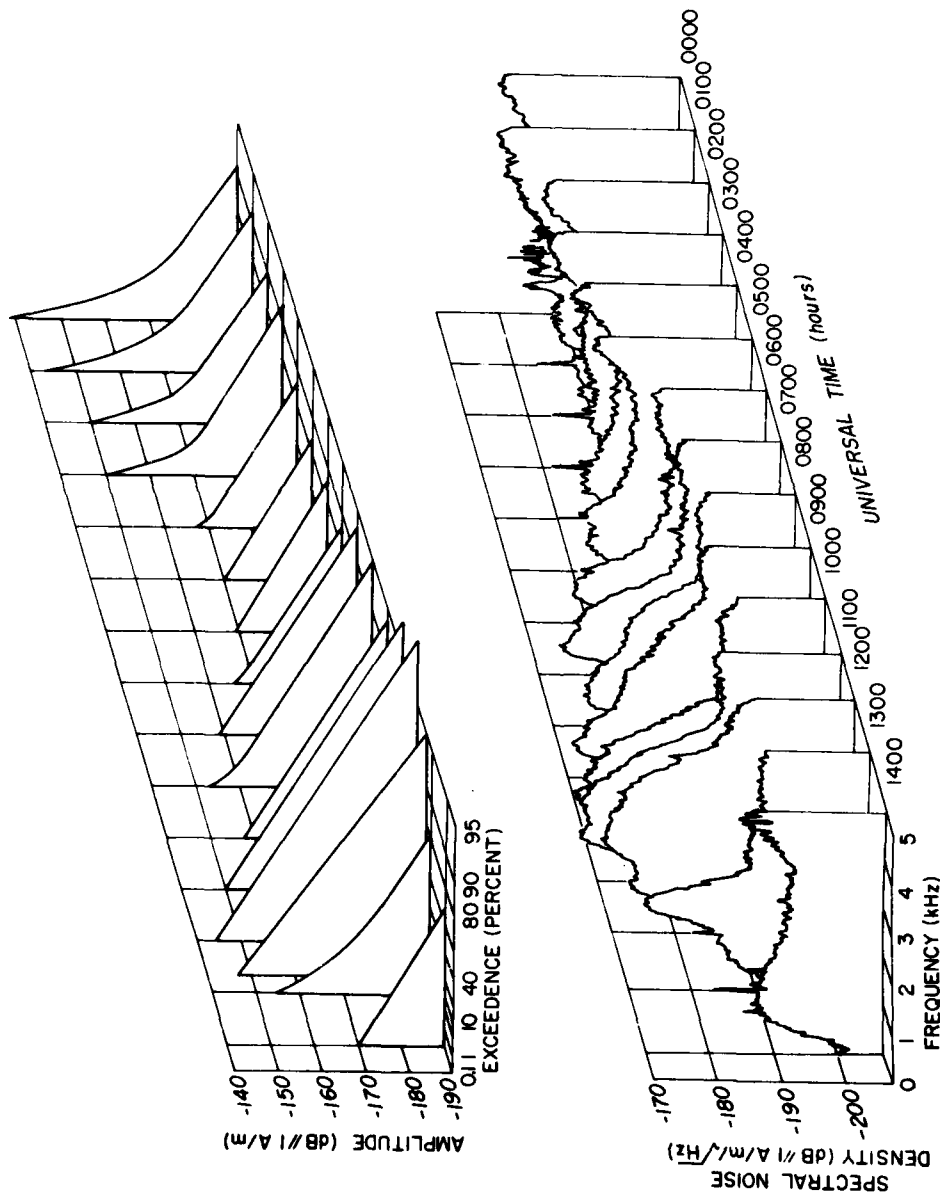
46

Fig. 34 — Comparison of APD and spectrum time histories during polar-chorus emissions recorded in Norway on 26 March 1978 (Fig. 31)

thunderstorm source regions; the filtering effect of the waveguide cutoff band on the emitted atmospheric impulse waveform is thus less important in determining the detected spectral noise density.

For the Norway spectra it is of interest to investigate the frequency of the spectral minimum and how it varies. The minimum frequency and its variation are shown statistically in Fig. 35 for the March 1978 data. Hourly spectra averaged over 10 minutes of data were analyzed throughout the 23-day interval to obtain the distribution of the minimum-noise-density frequency (the hatched area). As shown, the most probable minimum frequency occurs at 3.6 to 3.8 kHz, but at various times the minimum frequency was as low as 2.4 kHz or as high as 4.4 kHz. In general the values toward the upper end of this range (above about 4.2 kHz) occurred during the polar-chorus emissions.

Also shown in Fig. 35 is a distribution that can be considered as a statistical characterization of the bandwidth of the earth-ionosphere attenuation band. At a given frequency the percentage of the time that the spectral noise density was within 3 dB of the minimum noise density at that time is plotted. For example, between 2.8 and 3.0 kHz the noise spectral density was within 3 dB of the minimum value in about 83% of the samples. In
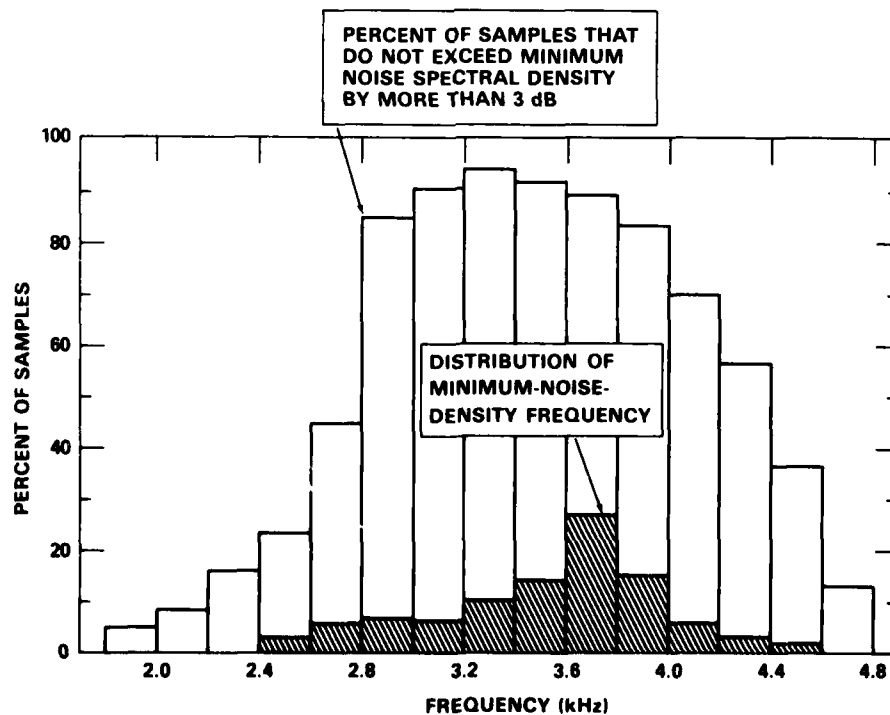

Fig. 35 — Histogram of two characteristics of spectral minimum, as recorded in Norway (March 1978, east-west loop)

48

general a communication system designed to operate within the attenuation band should use a frequency near the minimum spectral noise density to achieve maximum range [30]. The distribution of the minimum-noise-density frequency might imply that a frequency of about 3.7 kHz should be used; however, the bandwidth distribution favors a somewhat lower frequency near 3.3 kHz.

Because of the time and labor involved in obtaining the distributions, we have not similarly analyzed the Norway data taken in June 1978.

RECOMMENDATIONS

The data presented in this report should be helpful in dealing with questions relating to the effect of ambient noise on the performance of a 3-kHz communication system (such as transmitter sizing, maximum communication range, and waveform design). However, some results of this work suggest further measurements that would be of fundamental interest in the field of ionospheric physics. These measurements should address the following topics:

- *Propagation anisotropy.* The magnitude of the propagation anisotropy should be accurately measured, preferably by using a transmitting antenna. A horizontal grounded antenna on the Greenland icecap would permit a large current moment and would be located conveniently for distant propagation measurements. If a transmitting antenna were not available, further atmospheric noise measurements might be useful. Although a detailed analysis has not been carried out, it appears from Barr's paper [19] that the specific magnitude of the propagation anisotropy is very sensitive to ionospheric structure in the D region; hence anisotropy measurements might prove to be a valuable ionospheric diagnostic technique. In support of these measurements the nighttime attenuation rates at 3 kHz should be theoretically calculated.

- *Impedance of the earth-ionosphere waveguide.* Simultaneous measurements of the vertical electric field and the horizontal magnetic field would allow the impedance of the earth-ionosphere waveguide to the determined. Although accurate E-field measurements at 3 kHz are difficult, they are possible if sufficient care is paid to precipitation static effects and calibration procedures. Temporal and geographical variations of the impedance, and its measurement across the attenuation band, are of fundamental interest. The waveguide impedance should also be particularly sensitive to the structure of the waveguide boundary (the ionosphere).

ACKNOWLEDGMENTS

REFERENCES

1. R. Barr, "Some New Features of ELF Attenuation," Journal Atmos. Tem. Phys. 34, 411-420 (1972).

2. E.C. Field and M. Lewenstein, "Amplitude Probability Distribution Model for VLF/ELF Atmospheric Noise," IEEE Trans. Communications COM-26 (No. 1), 83-87 (Jan. 1978).

3. D. Middleton, "Statistical-Physical Models of Electromagnetic Interference," IEEE Trans. on EMC EMC-19 (No. 3), 106-127 (Aug. 1977).

4. J.E. Evans and A.S. Griffiths, "Design of a Sanguine Noise Processor Based Upon World-Wide Extremely Low Frequency (ELF) Recordings," IEEE Trans. Communications COM-22 (No. 4), 528-539 (Apr. 1974).

5. E.V. Appleton and F.W. Chapman, "On the Nature of Atmospherics — IV," Proc. Roy. Soc. 158A, 1-22 (1937).

6. A.D. Watt and E. Maxwell, "Characteristics of Atmospheric Noise From 1 to 100 Kc," Proc. IRE 45, 757-794 (June 1957).

7. J. Heirtzler, D. Nichols, and R. Santirocco, "Some Observations of the Geomagnetic Fluctuation Spectrum at Audio Frequencies," J. Geophysical Research 65 (No. 8), 2245-2547 (Aug. 1960).

8. J.B. Wilcox and E. Maple, "Audio-Frequency Fluctuations in the Geomagnetic Field," J. Geophysical Research 65 (No. 10), 3261-3271 (Oct. 1960).

9. E.L. Maxwell and D.L. Stone, "Natural Noise Fields from 1 cps to 100 kc," IEEE Trans. Ant. and Prop. 11, 339-343 (May 1963).

10. G. Gustaffson, A. Egeland, and J. Aarons, "Audio-Frequency Electromagnetic Radiation in the Auroral Zone," J. Geophysical Research 65 (No. 9), 2749-2758 (1960).

11. M.J. Rycroft, "Some Observations of Background Electromagnetic Radiation Near 5 kc/s," in Proceedings of Conference on MF, LF and VLF Radio Propagation, IEEE (London), 1967.

12. S. Westerlund, Report for Kiruna (Sweden) Geophysical Observatory under contract AF 61(052)-678, 1966; curves from this report are displayed in Ref. 13.

13. K.L. Feltham, "The Effect of Sunrise and Sunset on ELF and VLF Radio Noise," Ph.D. Thesis, University of London, Jan. 1968.

14. R.A. Helliwell, Whistlers and Related Ionospheric Phenomena, Stanford University Press, 1965.

15. M. Hayakawa, Y. Tanaka, and J. Ohtsu, "Satellite and Ground Observations of Magnetospheric VLF Hiss Associated with the Severe Magnetic Storm on May 25-27, 1967," J. Geophysical Research 80 (No. 1), 86-92 (Jan. 1975).

16. A.D. Watt, *VLF Radio Engineering*, Oxford, Pergammon Press, 1967.

17. A.G. Jean, H.E. Taggart, and J. Wait, "Calibration of Loop Antennas at VLF," J. Res NBS-C 65 (No. 3), 189-193 (July 1961).

18. E. Maxwell, D.L. Stone, R.D. Croghan, L. Ball, and A.D. Watt, "Development of a VLF Atmospheric Noise Prediction Model," Westinghouse Georesearch Laboratory Report 70-1H2-VLFNO-R1, 30 June 1970 (AD 902023).

19. R. Barr. "The Propagation of ELF and VLF Radio Waves beneath an Inhomogeneous Anisotropic Ionosphere," J. Atmos. Terr. Physics 33, 343-353 (1971).

20. D.G. Deeks, "D-Region Electron Distributions in Middle Latitudes Deduced from the Reflexion of Long Radio Waves," Proc. Roy. Soc. A291, 413-437 (1966).

21. S.O. Rice, "Properties of a Sine Wave Plus Random Noise," Bell System Tech. J. 27, 109-157 (Jan. 1948).

22. A.P. Ciervo, M. Lewenstein, and E.C. Field, "VLF Noise Statistics and Processing Under Disturbed Conditions," Pacific-Sierra Research Corp. Report 601, Jan. 1976.

23. B. Carnahan and J. Wilkes, *Digital Computing and Numerical Methods*, Wiley, 1973.

24. D. Middleton, *An Introduction to Statistical Communication Theory*, McGraw-Hill, 1960, Appendix 1.

25. S. Rappaport and L. Kurz, "An Optimal Nonlinear Detector for Digital Data Transmission Through Non-Gaussian Channels," IEEE Trans. Comm. COM-14, 266-274 (June 1966).

26. J.R. Davis and W.D. Meyers, "ELF Atmospheric Noise Excision by Wideband Clipping," Radio Science 11 (No. 12), 991-999 (Dec. 1976).

27. J. Goldstein, W.D. Meyers, and J.R. Davis, "ELF Nonlinear Processing Experimental Measurements, Part 3 — Synoptic Sample of Diurnal and Seasonal Noise Variation in Italy," NRL Memorandum Report 3534, July 1977.

28. E. Ungstrup and I. Jackerott, "Observations of Chorus Below 1500 Cycles per Second at Godhavn, Greenland, from July 1957 to December 1961," J. Geophysical Research 68 (No. 8), 2141-2146 (1963).

29. L. Harang, "VLF-Emissions Observed at Stations Close to the Auroral Zone and at Stations on Lower Latitudes," J. Atmos. Terr. Phys. 30, 1143-1160 (1968).

30. R. Dinger, W. Meyers, and J. Goldstein, "Experimental Investigations of Transmission, Propagation, and Reception of 3-kHz Electromagnetic Waves for Tactical Communication Applications," NRL Report 8376, Feb. 1980.

Appendix A

ELF/VLF PROPAGATION EQUATIONS

This appendix discusses briefly the equations that describe wave propagation near 3 kHz in the earth-ionosphere waveguide.

Wait* was the first to derive waveguide modal equations for ELF and VLF propagation. The transverse magnetic field strength H_ϕ on the earth's surface at a distance d from a dipole source I_0 is given by

$$H_\phi = \frac{I_0 \, e^{-i \, 3\pi/4}}{\sqrt{\lambda a \, \sin(d/a)}} \sum_{n=0}^{\infty} \delta_n \, S_n^{3/2} \, e^{-ik \, S_n d} , \qquad (A1)$$

where λ is the wavelength, $k = 2\pi/\lambda$, and a is the radius of the earth and where

$$S_n = \sqrt{1 - C_n^2}$$

and

$$\delta_n = \frac{i2kh(e^{i2khC_n} + R_2) e^{i2khC_n}}{(\partial W/\partial C)_{C=C_n}} ,$$

in which

$$W = (e^{i2khC} - R_1)(e^{i2khC} + R_2) + R_3 R_4$$

and in which C_n is a solution of the equation $W = 0$, n is the ionospheric reflecting height, and R_1 through R_4 are ionospheric reflection coefficients described in more detail by Wait*. The index n labels the various waveguide modes that propagate in the earth-ionosphere waveguide. A particular ionospheric model, typically with a height-dependent electron density and collisional frequency profile, affects the computed field strength through the values of R_1 through R_4. Barr [19] has described the technique by which the reflection-coefficient values can be derived from the features of an ionospheric model.

---

*J.R. Wait, *Electromagnetic Waves in Stratified Media*, Pergamon, 1962.

Equation (A1) can be written in the form

$$H_\phi = \frac{I_0\, e^{-i\, 3\pi/4}}{\sqrt{\lambda a\, \sin\,(d/a)}} \sum_{n=0}^{\infty} \Lambda_n\, e^{(-\,\alpha_n\,-\,i\beta_n)d}\,. \qquad (A2)$$

The factors δ_n and S_n have been collected in a mode excitation factor Λ_n, and an attenuation rate α_n and propagation constant β_n have been defined:

$$\alpha_n = \frac{2\pi f}{c}\, \text{Im}\,(S_n) \qquad (A3)$$

and

$$\beta_n = \frac{2\pi f}{c}\, \text{Re}\,(S_n), \qquad (A4)$$

where Im (...) and Re (...) refer to the imaginary and real parts respectively. The units of α_n are nepers per unit distance. Commonly, the attenuation rate is expressed in dB per unit distance; if the megameter (Mm) is selected as a convenient unit of distance, the attenuation rate in dB/Mm, denoted $\overline{\alpha}_n$, is

$$\overline{\alpha}_n = (20\, \log_{10} e)\, \alpha_n \qquad (A5)$$

or

$$\overline{\alpha}_n = 0.182\, f\, \text{Im}\,(S_n) \quad \text{dB/Mm.} \qquad (A6)$$

Our principal interest in is the value of $\overline{\alpha}_n$. Barr [19] has computed the variation of $\overline{\alpha}_n$ with frequency for a realistic ionospheric model, and in Fig. A1 we have reproduced a plot from Barr's paper. Shown are the attenuation rates for the $n = 0$ and $n = 1$ modes for propagation in north-south, east-to-west, and west-to-east directions. The attenuation rates for modes with $n > 1$ are much greater than the already large values evident in Fig. A1. The peak in the attenuation rate $\overline{\alpha}_0$ occurs near 3 kHz, at which frequency $\overline{\alpha}_0$ is about 60 dB/Mm; it is this high attenuation rate that produces the low values of atmospheric noise given in this report. Figure A1 clearly indicates that at 3 kHz only the mode $n = 0$ needs to be retained in Eq. (A2). Hence at 3 kHz the amplitude of the transverse magnetic field produced by an atmospheric impulse can be written simply as

$$|H_\phi| = \frac{I_0\, \Lambda_0\, e^{-\alpha_0\, d}}{\sqrt{\lambda a}\, \sqrt{\sin\,(d/a)}}\,. \qquad (A7)$$
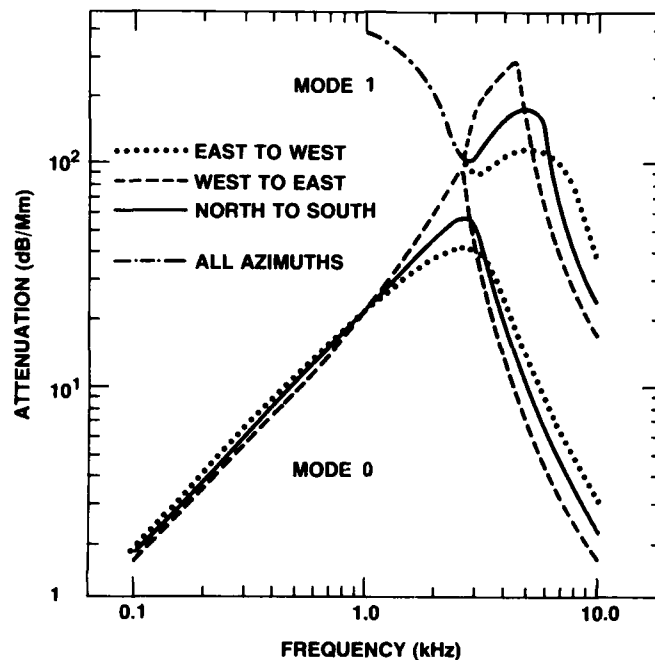
Fig. A1 — Computed values of the attenuation
coefficient (from Ref. 19)

A large propagation anisotropy is evident from the curves in Fig. A1. The dependence
of attenuation rate on direction of propagation is caused by the influence of the direction
of the earth's magnetic field on the ionospheric reflection coefficients in Eq. (A1). Experi-
mental evidence for this propagation anisotropy is offered by the noise data presented in
this report. (Appendix C will discuss how the simple functional form of (A7) can be used to
derive an approximate relationship for the attenuation-coefficient anisotropy from the
experimental data.)

Appendix B

STATISTICAL ANALYSIS OF EAST-WEST PROPAGATION ENHANCEMENT

This appendix discusses the statistical significance of the difference between the night-time east-west and north-south noise densities recorded in Norway during March 1978. The question is: Using the appropriate test statistic, at what confidence levels are the hourly differences between the east-west and north-south noise densities significant?

Define $\langle d \rangle = \langle H_{EW} - H_{NS} \rangle$ as the mean difference between the east-west and north-south spectral noise densities, where the averages are computed over the 23 days of data at a given hour each day, and define S_d as the standard deviation of the difference. As shown by Fraser*, if H_{EW} and H_{NS} are independent variables, then the test statistic defined by

$$T = \frac{\langle d \rangle}{S_d / \sqrt{n}} , \tag{B1}$$

where n is the number of samples, has a Student's t distribution with $n - 1$ degrees of freedom, denoted $t(n - 1)$.

Table B1 — Compilation of statistical variables
(defined in the text) for east-west and north-south
noise spectral density difference for data
recorded in Norway in March 1978

Hour (UT)	n	$\langle d \rangle$ (dBH)	S_d	T	p
1600	21	−0.52	2.18	1.10	0.14
1700	23	−0.33	2.25	0.69	0.25
1800	20	1.35	2.72	2.22	0.019
1900	22	3.34	4.59	3.41	1.3×10^{-3}
2000	20	3.55	2.30	6.90	7.1×10^{-7}
2100	22	3.89	2.66	6.85	4.2×10^{-7}
2200	22	3.07	3.30	4.36	1.4×10^{-4}
2300	19	2.34	2.23	4.57	1.2×10^{-4}
2400	20	2.22	2.46	4.04	3.5×10^{-4}
0100	20	1.55	2.29	3.03	3.4×10^{-4}
0200	21	1.52	2.47	2.82	5.2×10^{-3}
0300	20	0.60	2.38	1.13	0.14
0400	19	−0.55	3.00	0.80	0.22

*D. Fraser, *Statistics· An Introduction*, 1958.

Table B1, for the hours 1600 to 0400, shows the calculated value of $\langle d \rangle$, S_d, and T for the data recorded in Norway in March 1978. With use of a programmable calculator, the probability p of observing the measured value of T in a $t(n - 1)$ distribution purely by chance was computed and is given in the last column of Table B1. The confidence level, which is in percent, for each hourly difference is 100p.

Confidence levels of 1.0% or less are usually considered to be sufficient for testing a hypothesis. Table B1 shows that the mean difference becomes significant below the 1.0% level at 1900 UT (approximate local sundown) and stays below this level until 0300 UT. At the maximum-difference times of 2000 and 2100 UT the difference is significant at approximately the 10^{-4}% level. Table B1 clearly indicates that the observed differences in the east-west and north-south noise spectral densities are statistically significant.

Appendix C

DERIVATION OF ATTENUATION-COEFFICIENT
ANISOTROPY FROM EXPERIMENTAL AMBIENT-NOISE DATA

This appendix discusses how approximate values of the anisotropy of the attenuation coefficient for the mode $n = 0$ can be derived from experimental ambient-noise data for comparison with theoretical calculation. The calculations in this appendix show that the approximations required for this comparison allow only a qualitative judgment of the anisotropy.

DERIVATION OF THE EQUATIONS

For a loop receiver the time-averaged voltage output in a narrow bandwidth can be approximated as follows, using Eq. (A7):

$$\bar{V} = C \sqrt{\sum_{m=1}^{N} \left[\frac{I_{0m} \Lambda_{0m} e^{-\alpha_{0m} d_m}}{\sqrt{\sin (d_m/a)}} \cos \theta_m \right]^2}, \tag{C1}$$

where m is an index for each thunderstorm cell, N is the total number of thunderstorm cells, I_{0m} is the (time and space) average current moment in the mth cell, Λ_{0m} is the (time and space) average excitation factor for the mth cell, α_{0m} is the average path attenuation rate from the mth cell to the receiver, d_m and θ_m are the distance and azimuthal bearing respectively of the mth cell, and C is a receiver gain constant (into which the $\sqrt{\lambda a}$ factor in Eq. (A7) has been absorbed). This technique of summing incoherently the average noise powers emitted by thunderstorm cells to obtain a total noise power at a receiving site was first used by Maxwell et al. [18] for VLF noise prediction. The area or extent of a cell depends on the rigor with which one attempts to model the noise. To extract an average attenuation coefficient, we must in fact assume that only a single cell contributes substantially to the measured noise; rather than "cell" a better terminology might be "major thunderstorm area" in this case.

Therefore, for an a north-south-oriented loop whose response is assumed to be dominated by a single major thunderstorm area, the output voltage can be approximated by

$$\bar{V}_N = \frac{C I_{0N} \Lambda_{0N} e^{-\alpha_{0N} d_N}}{\sqrt{\sin (d_N/a)}} \cos \theta_N. \tag{C2}$$

Likewise, the east-west-oriented loop is assumed to have an output voltage given by

$$\overline{V}_E = \frac{C\,I_{0E}\,\Lambda_{0E}\,e^{-\alpha_{0E}\,d_E}}{\sqrt{\sin\,(d_E/a)}}\;\cos\theta_E.\tag{C3}$$

These equations implicitly assume that the receiver is far enough from the thunderstorm area that a single distance and azimuthal bearing can be reasonably ascribed to it (that is, the transverse and radial extent of the thunderstorm area is small compared to the mean distance).

To combine Eqs. (C2) and (C3), we take the logarithm of both sides of the equations, subtract one from the other, and express the attenuation coefficients in dB/Mm (Appendix A):

$$\overline{\alpha_{0N}} - \frac{d_E}{d_N}\,\overline{\alpha_{0E}} = \frac{1}{d_N}\left\{20\log\left(\frac{I_{0N}\,\Lambda_{0N}}{I_{0E}\,\Lambda_{0E}}\right) + 20\log\left(\frac{\cos\theta_N}{\cos\theta_E}\right)\right.$$
$$\left. + 10\log\left[\frac{\sin\,(d_E/a)}{\sin\,(d_N/a)}\right] - 20\log\left(\frac{\overline{V}_N}{\overline{V}_E}\right)\right\},\tag{C4}$$

where the bar over α_0 indicates units of dB/Mm for the attenuation coefficient.

For comparison of measured and theoretical values of the attenuation coefficient anisotropy, we assume that a receiving site is established where a single distant major thunderstorm area can be identified that is at a bearing near $\theta_N \approx 0$, so that it dominates the north-south response, and where a single distant major thunderstorm area is at a bearing near $\theta_E \approx 0$, so that it dominates the east-west response. Such a site would be selected with the assistance of thunderstorm distribution maps [18], from which the values of θ_N, d_N, θ_E, and d_E would be obtained. Long-term measurements of $\overline{V}_N$ and $\overline{V}_E$ would then be taken. Apart from the attenuation coefficients themselves, the only remaining unknown in Eq. (C4) is the ratio of the products of the source moment I_0 and the excitation factor Λ_0. Estimates of this ratio can possibly be obtained from the data base incorporated into the VLF noise model of Ref. 18, or perhaps two auxiliary measurement stations positioned near the major thunderstorm areas would permit an experimental measurement of the ratio. (For comparing the data in this report, we will assume that the ratio is unity, as justified in the next section.) Equation (C4) thus yields a relation between $\overline{\alpha}_{0N}$ and $\overline{\alpha}_{0E}$ that can be compared with a theoretical calculation.

COMPARISON WITH DATA IN THIS STUDY

Figure 12 shows that the Tromsø, Norway, site in March satisfies reasonably well the requirement for one distant dominating thunderstorm area along east-west and north-south directions. (The thunderstorm areas in South America are assumed to contribute a negligible amount to $\overline{V}_E$ on the basis of Barr's [19] calculations that show a much higher attenuation rate for west-to-east propagation as compared to east-to-west propagation.)

From Fig. 12 the following values are taken: $d_N = 8$ Mm, $\theta_N = 10°$, $d_E = 10$ Mm, and $\theta_E = 8°$. The ratio $I_{0N} \Lambda_{0N}/I_{0E} \Lambda_{0E}$ is set equal to unity, for the following reasons. Both thunderstorm areas are equatorial regions, which produce thunderstorms that are expected to be similar in such characteristics as average source strength. The excitation factors Λ_{0N} and Λ_{0E} are known [16] to depend on magnetic-field orientation, ground conductivity, and ionospheric structure; all of these factors are similar in both locations.

Hence in this case Eq. (C4) becomes (using $a = 6.4$ Mm)

$$\overline{\alpha_{0N}} - 1.25 \,\overline{\alpha_{0E}} = 0.12 \,(0.23 - 20 \log \frac{\overline{V}_N}{\overline{V}_E}).$$

From Table B1 the quantity $20 \log (V_N/V_E)$ is equal to $- 3.9$ dB at 2100. Thus the experimental data imply that the attenuation coefficients are related by

$$\overline{\alpha_{0N}} = 0.50 + 1.25 \,\overline{\alpha_{0E}}.$$

END

DATE
FILMED

9 80

DTIC

SUPPLEMENTARY

INFORMATION

ERRATA FOR NRL REPORT 8413

Recently, you were sent a copy of NRL Report 8413, "Experimental Measurements of Ambient Electromagnetic Noise from 1.0 to 4.0 kHz," by Robert J. Dinger, William D. Meyers, and John R. Davis, dated 31 July 1980. This report had two errors:

- The curve labels for Figure 27 on page 40 are incorrect. *All* curves are for data taken with the North-South loop. The curves with solid circles are for data recorded in June, 1978; the curves with squares are for data recorded in March/April 1978.

- Equation (12) should be

$$H(R) \approx \frac{e^{-\alpha R}}{\sqrt{\sin(R/a)}}$$